Structures 54 (2023) 330–347

Contents lists available at ScienceDirect

Structures

journal homepage: www.elsevier.com/locate/structures

MSA-based seismic fragility analysis of RC structures considering soil nonlinearity effects and time histories compatible to uniform hazard spectra

Srijit Bandyopadhyay [a,b,*], Y.M. Parulekar [a,b], Aniruddha Sengupta [c]

[a] Homi Bhabha National Institute, Mumbai 400094, India
[b] Reactor Safety Division, Bhabha Atomic Research Center, Mumbai 400085, India
[c] Department of Civil Engineering, Indian Institute of Technology, Kharagpur 721302, India

A R T I C L E I N F O

Keywords:
Fragility analysis
Ground motion simulation
Uniform hazard Response Spectra
Soil nonlinearity

A B S T R A C T

In the present study, an updated ground motion simulation framework based on spectral compatible time histories is proposed for the evaluation of seismic performance of mid-rise reinforced concrete structures with multi-stripe analysis (MSA) based probabilistic seismic hazard analysis. The seismic fragility functions are generated for two numbers of three storied instrumented test buildings of which one is founded on individual flexible footings and other one is a base isolated building. The fragility analysis is carried out for different performance levels under a series of input ground motions (IGMs) by considering uncertainty in soil structure interaction and uncertainty in ground motion. IGMs are obtained from the uniform hazard response spectrum (UHRS) with different return period thus conserving the frequency content of input motion during the scaling of high intensity earthquakes. The UHRS compatible synthetic time histories are applied at rock level and amplified surface motion obtained from soil amplification studies considering soil nonlinearity are applied to the buildings supported on soil springs. Nonlinear time history analysis is performed by modelling hysteretic characteristic of columns using modified Takeda model. The fragility curves obtained from the proposed methodology are compared with that using simple scaling of accelerograms generally performed in literature. The proposed technique gives conservative result for structure with individual flexible footings while no marked differences are observed for base isolated structure.

1. Introduction

Most of the old low to medium rise RC framed buildings are not efficiently designed to withstand high level of seismic excitation and thus do not cater the more stringent latest seismic criteria. Development of fragility curves for such structures at different performance levels is a pre-requisite for seismic vulnerability assessment [4,22,25,43,50,54]. The fragility curve represents a continuous relationship between probability of exceedance (POE) of a pre-defined limit state of the structure and ground motion intensity measure. The assessment of structural collapse requires efficient and accurate analytical model to represent the nonlinear behavior of the structure and realistic scaling of input ground motions.

The central philosophy of the fragility estimation is to take into account the uncertainty and randomness of variables used in the analysis for earthquake loads. Typically, the most dominant contributors of the uncertainty in the seismic analysis are the input ground motion variability and uncertainty in the soil parameters [47]. The uncertainty in the soil parameters gives rise to uncertainty in soil-structure interaction (SSI) which is an important part of seismic analysis of structures. When the seismic waves travel through the soil layer, a modification of the frequency content and amplitude of the ground motion is observed due to the heterogeneity of the soil layer and soil nonlinearity.

Most of the researchers [21,40,49,58] in the past few decades considered that the underlying foundation soil is represented as an equivalent spring during performance of non-linear time history analysis (NLTHA) of the structure without considering the effect of soil nonlinearity. The main drawback of the above-mentioned procedure is that, the variation of the characteristics of seismic motion with varying soil nonlinearities and intensity of input motion is eliminated. Pitilakis et al.

* Corresponding author.
E-mail addresses: srijit@barc.gov.in (S. Bandyopadhyay), yogitap@barc.gov.in (Y.M. Parulekar), sengupta@civil.iitkgp.ac.in (A. Sengupta).

https://doi.org/10.1016/j.istruc.2023.05.076
Received 12 January 2023; Received in revised form 16 May 2023; Accepted 19 May 2023

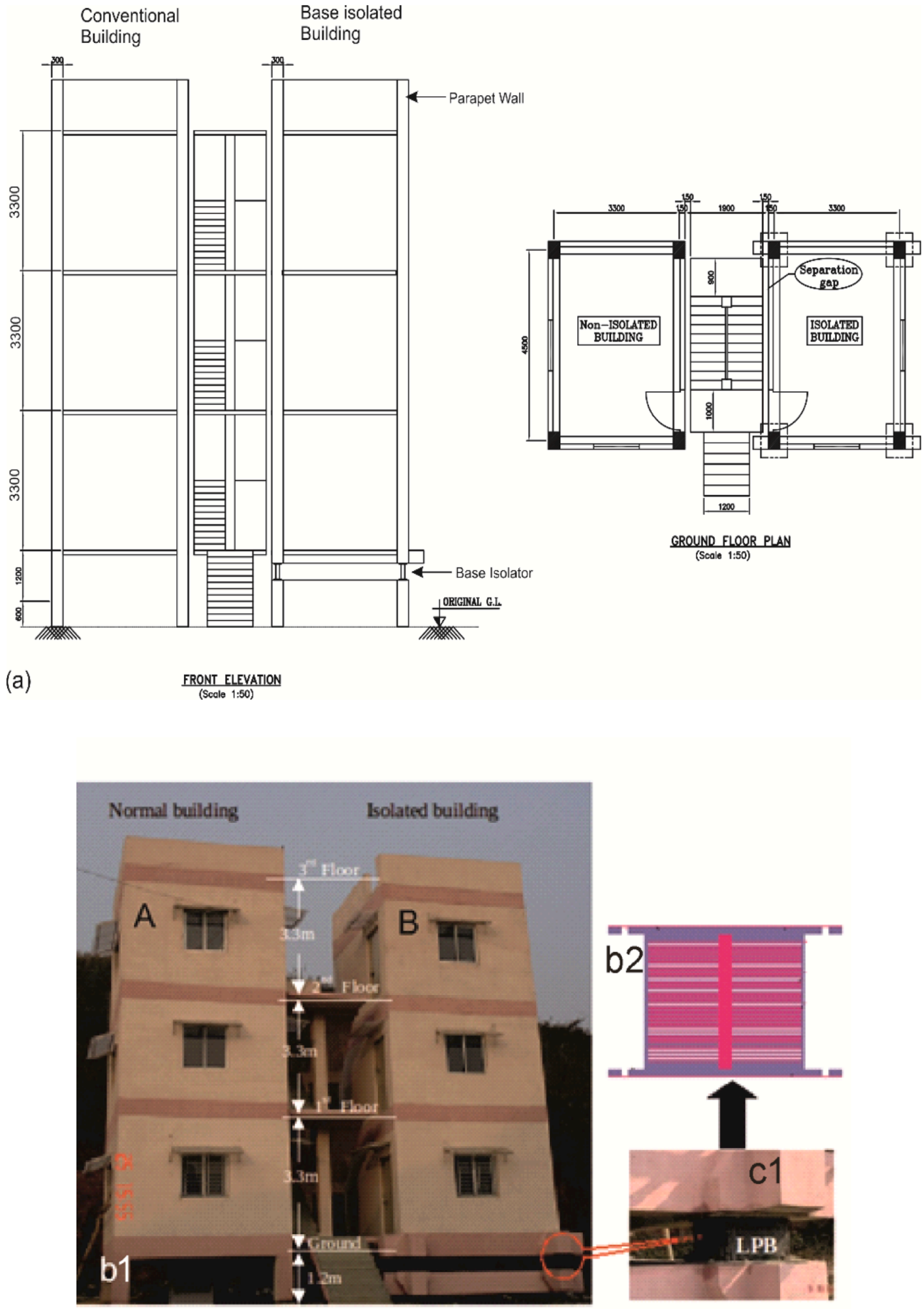

(b)

Fig. 1. (a) Plan and elevation of conventional and isolated building showing position of isolators; (b) Isometric view of the buildings located in Guwahati. (adopted from Bandyopadhyay et al. [11].

[45] considered the SSI effect during the study of the generation of fragility curves of the buildings by applying the direct one-step approach, in which inertial and kinematic interactions were accounted simultaneously and soil was modelled using 2D plane strain soil element. He reported that considering SSI effect increases the vulnerability values. Karapetrou et al. [31] also generated fragility curves of a structure with consideration of the SSI and he also reported similar phenomenon. Khosravikia et al. [33] represented the foundation soil as an equivalent spring and performed the fragility analysis for different types of structures. He reported that building resting on soft soil has less effects in seismic vulnerability compared to the fixed base structure. Various researchers [5,12] reported that free-field motion was amplified with respect to bed rock motion during site response analysis (SRA) of the soft soil column. However, Lopez-Caballero et al. [37] reported that free field motion was de-amplified during soil response analysis. This shows that hysteresis behaviour of the soils plays an important role in

the response of the free field motion.

The key parameters to measure the uncertainties is using correlation of demands and capacities for evaluation of structural response under earthquake load. These demand v/s capacity correlation for a structural system subjected to series of ground motions can be determined using an analytical method introduced by Vamvatsikos and Cornell [60] and later extended in 2005 [61,62], which is called as Incremental Dynamic Analysis (IDA). IDA is a parametric non-linear dynamic analysis method, which is used to estimate the structural performance under several input ground motions (IGMs) and it includes the development of one or more curves of a specific damage measure (DM) (i.e., maximum story drift as a percentage) versus an intensity measure (IM) of the earthquake (peak ground or 1st mode spectral acceleration). The represented input motions are selected from the strong motion database and scaled linearly to get structural response from linear range to plastic state. Researchers [17,36] pointed out a key drawback of the IDA technique that this method is unable to represent the actual frequency content of the motion during high intensity scaling and IDA is computationally cumbersome. Another most common procedure, used for generating fragility curves by obtaining relationship between DM and IM based on IGMs, is multi-stripe analysis (MSA). Scozzese et al. [51] investigated the effectiveness of MSA procedure with a series of parametric studies on a three-story frame. Iervolino and Cornell [28] pointed out that different earthquakes with same PGA produced different response spectra. Hence, the point of concern is obtaining representative input ground motions for study area, where mild to major recorded ground motion are not available or available with the exception of a few.

In order to fill this gap area, a realistic and proper way of obtaining the IGMs from the range of mild to severe ones is required to be generated by conducting probabilistic seismic hazard analysis (PSHA) of the site. Hence, there is a pressing need to propose a novel methodology to generate fragility curves using these realistically generated IGMs. In the present work, a new technique to carry out multi-stripe analysis for evaluation of fragility curves using PSHA with the local site effects which includes realistic scaling of ground motion as well as soil uncertainty, is proposed. The novelty of the study is that the scaling of IGMs is performed by generating UHRS of higher return period (RP) at the study area and these representative ground motions obtained by UHRS are used for generating fragility curves. The important motive that the soil and geology change the characteristics of the ground motion as the intensity increases is thus taken care in fragility estimation of the structures.

In the present work, failure probabilities of two RC framed structures of which one is founded on individual flexible footings and other one is a base isolated structure, are estimated by performing fragility analysis using MSA technique for different limit states. The buildings are located in Guwahati region of India and hence ten different site-specific response spectra of Guwahati region with ten dissimilar attenuation relations are obtained by performing PSHA for Assam region [10] and scaling of these spectra is done using return period varying from 100 years to 50000 years. The UHRS compatible synthetic time histories are applied at rock level and amplified surface motion obtained from soil amplification studies considering soil nonlinearity effect are applied to the buildings supported on soil springs. Nonlinear Time History analysis (NLTHA) is performed by considering structural nonlinearity using modified Takeda model for the columns. Fragility curves using MSA are then estimated for different performance levels of the structures with above-mentioned new scaling methodology considering soil uncertainty. Lastly, the fragility curves obtained from this proposed new technique are compared with those obtained by conventionally carried out linear scaling of synthetic ground motions compatible to the above mentioned ten site specific spectra of 100 yrs RP considering soil uncertainty.

Table 1
Geometric and material data of the buildings.

No of storeys	G + 3
Total height	12.9 m
Floor height	1.8 m (Foundation to plinth level) and 3.3 m (Typ)
Beams	B1 (250 mm × 350 mm) (Along shorter span) and B2 (250 mm × 450 mm) (along longer span)
Columns	C1 (300 mm × 400 mm)
Equivalent X direction beams along shorter span	250 mm by 350 mm
Equivalent Y direction beams along shorter span	250 mm by 400 mm
Concrete Strength f_{ck},	25 MPa, Strain at peak stress = 0.002, failure strain = 0.0094
Yield strength of steel fy	415 MPa, Proof strain = 0.002
Density of infills	1800 kg/m^3
Young's Modulus of infill (MPa)	1500
Compressive strength of infill (MPa)	3

2. Description and FE modeling of structures

Two instrumented three-storied buildings are considered for the study, one is regular structure founded on individual flexible footings and other one is base isolated structure placed over a lead rubber base isolator (LRB) as shown in Fig. 1. The first structure is referred further as flexible base non-isolated structure (FBNIS) and the other structure is referred as Flexible base Base Isolated structure (FBBIS). These structures are constructed in Guwahati region of India to gather real time earthquake data and study their response during real earthquakes. Buildings are designed based using Indian standard seismic code [14]. The measurement of real time earthquakes and numerical simulation of the FBNIS subjected to these earthquakes with linear dynamic analysis is explained by Bandyopadhyay et al. [11]. Moreover, the nonlinear modelling of base isolators for the FBBIS is also explained in details by Bandyopadhyay et al. [11] along with numerical simulation of FBBIS subjected to very large earthquake. In the present work, same buildings are considered for fragility evaluation by performing series of Linear Time history analysis for lower-level earthquakes and performing NLTHA for higher level earthquakes considering both the structural and soil nonlinearity. Details of modeling of the structures is explained henceforth.

2.1. Superstructure modelling

The FBNIS shown in Fig. 1 consists of 4 columns and each column is founded over a flexible individual isolated footing. The FBBIS has additional base isolators attached at the plinth level. Both the buildings have brick infill masonry in their external walls and these infills are considered to be prevented from out of plane collapse when subjected to large earthquake by properly retrofitting them by strips of steel or carbon fibers. Thus, considering this postulation of prevention of out-of-plane failure of brick walls, the brick wall modeling is incorporated as an equivalent strut, as per the guidelines given in IS-1893 (part1), details of which are explained by Bandyopadhyay et al. [11]. The geometric data of the building is presented in Table 1 and c/s details of beams and columns are shown in Table 2.

All the beam and column members of both the structures are modelled in MIDAS FEA NX using the inelastic beam element. This inelastic beam is classified in two types in the FEA software, one is lumped type and other one is distributed type. In present analysis, lumped type inelastic beam element is adopted. This element is a beam element which is assigned inelastic hinge properties and it basically comprises an envelope curve to represent the global behavior of the complete cross-section in terms of moment–curvature. The formulation is thus represented by inserting inelastic rotational springs of non-dimensional lengths at both ends of beam element, which can deform plastically,

Table 2
C/S details of the sections.

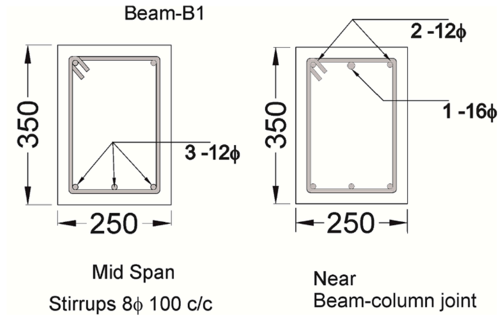

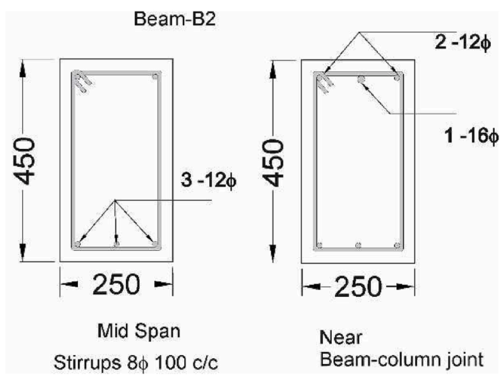

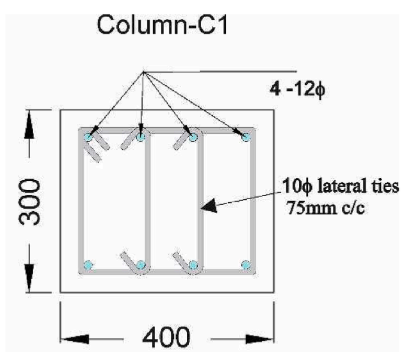

into the beam element. The remaining parts other than the lumped type inelastic hinges are modelled as an elastic beam. The modeling of the plastic hinges is thus carried out by including a zero-length element link between two adjacent beam elements, in which a constitutive law is defined. Moreover, when yield occurs due to irregular cyclic load such as seismic load the non-linear cyclic behavior of the RC frame structure is incorporated using hysteresis model at the same location of hinges. Thus, the inelastic beam element is capable of modeling the respective behavior of the structural system in macro way.

For beam members of the framed structure model, the axial load effects are ignored as the rigid floor diaphragm effect is considered and moment curvature characteristics are evaluated as shown in Fig. 2. It is observed from the orientation of the columns in Fig. 1 (a) that the structure is more flexible in X direction and the peak load capacity is lesser in X direction. The effect of axial load on plastic hinges is considered using a P-M interaction diagram for each RC section of the columns and the moment - curvature (M-ϕ) curves for the columns of ground floor, first floor, second floor and third floor in X direction are shown in Fig. 3. The structures are detailed as per IS 13920 (1993) ductile detailing. The detailing provisions specified in IS 13920 (1993) exclude the possibility of shear failure of beam-column joint hence no shear hinge formation is considered in the analysis. Such detailing of the structure ensures confinement effect in the concrete columns and beams hence the Kent and Park [32] model for confined concrete is used for modelling the concrete within the stirrups for the column and beam members. Large bar-slip decreases the joint shear strength, which cause early shear failure of the beam-column joint. However, due to the ductile detailing provision used for the joints the beam-column joints are assumed to be rigid and strong enough to avoid any premature failure before forming a mechanism by the failure of other members (see Fig. 4).

For performing nonlinear dynamic analysis, the appropriate hysteresis model is adopted and this is achieved by the proper optimization and calibration of the parameters defining the hysteresis model which in the present work is input using Takeda Trilinear hysteresis model. This

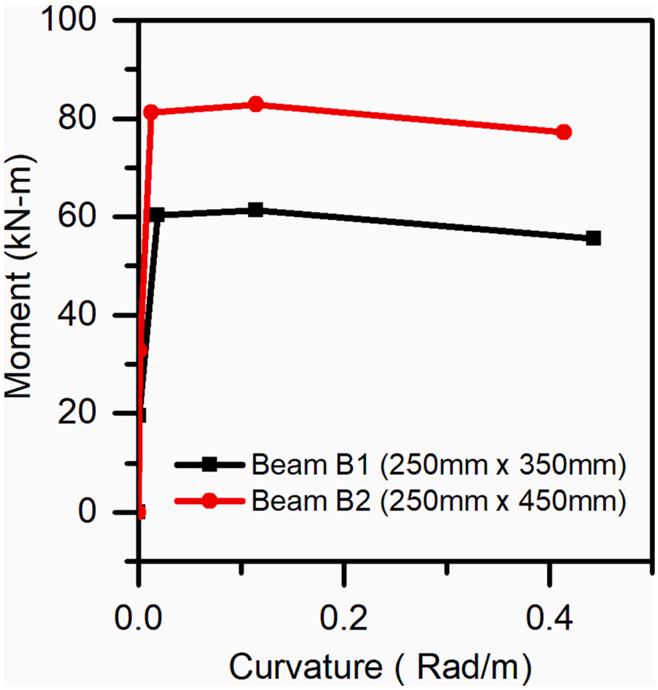

Fig. 2. M-ϕ curves for beams.

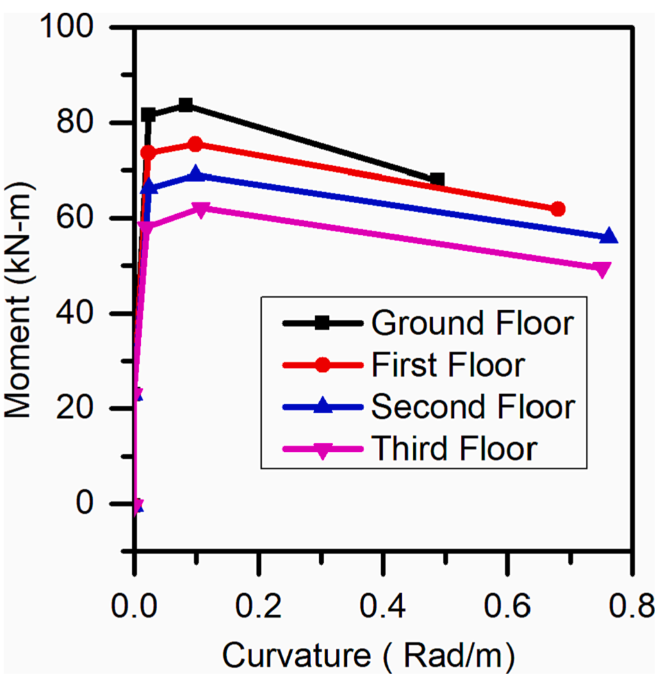

Fig. 3. M-ϕ curves for Columns in X direction.

model is widely used in seismic simulation of structures due to few control parameters and precise physical meanings.

Fig. 4 shows the schematic representation of the modified Takeda model. It illustrates that the initial stiffness is k_0, and post yielding stiffness factor is represented by r. The rate at which the displacement ductility dependent unloading stiffness decreases is stated as parameter, α. The stiffness degradation thus depends upon the ratio of yield curvature to maximum curvature experienced by the element during the cyclic loading. The reloading stiffness factor β, gives the point on the backbone curve where a current excursion will intersect the previous excursion curve. The above explained input parameters are selected

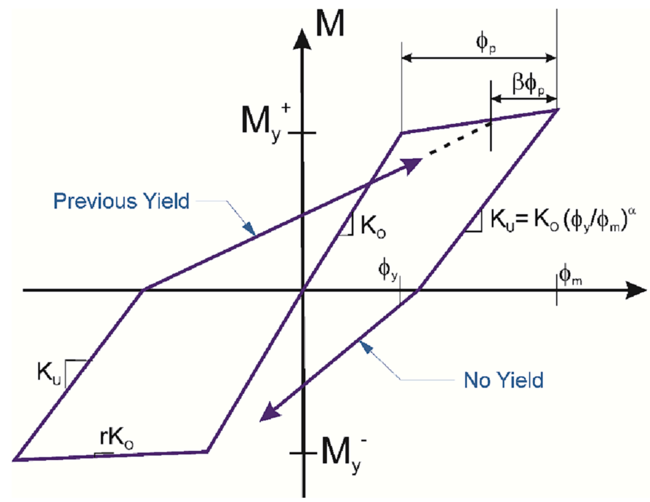

Fig. 4. Schematic representation of Modified Takeda model.

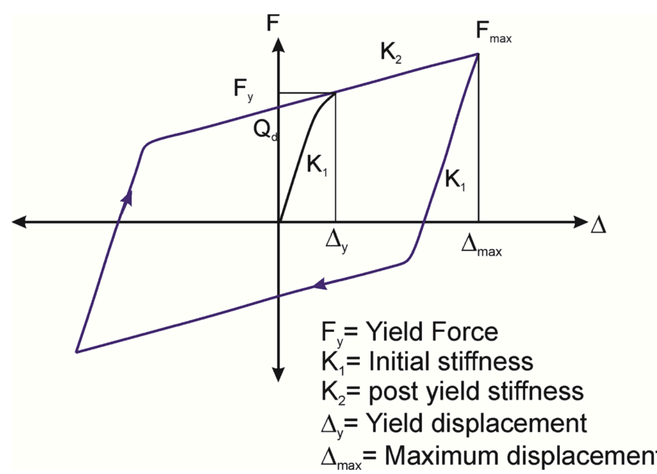

Fig. 5. Schematic diagram of the Bouc-Wen Hysteretic.

based on “Takeda Fat” (TF) hysteresis and “Takeda Thin” (TT) hysteresis. TF hysteresis is generally chosen for beam members and assumes that $\alpha = 0.3$ and $\beta = 0.6$ while TT hysteresis assumes $\alpha = 0.5$ and $\beta = 0$ to represent the energy dissipation expected for members with high axial load (e.g. - columns). In the present work, the columns do not have very high axial load hence unloading stiffness calculation coefficient (α) is considered as 0.4 and β is considered as 0 for the analysis. The other control parameters including r and initial stiffness (K_O) of moment curvature curve of modified Takeda model for the columns are already represented in Fig. 3. In FBBIS, lead plugs are installed to dissipate energy. Here, base isolator characteristics are modeled using bilinear Bouc-Wen Hysteretic model as shown in Fig. 5. The nonlinear link element is used in FEA NX software to model the base isolator. The isolator parameters which are reported in Bandyopadhyay et al. [11], are as follows, initial stiffness $K_1 = 7.1$ kN/mm, yield stiffness, $K_2 = 0.82$ kN/mm, yield displacement, $\Delta_y = 4.1$ mm, Characteristic strength $= Q_d = 26$ kN, and yield force $F_y = 29$ kN.

The maximum force of the isolator, F_{max} is the force taken by the isolator (192 kN.) at its design maximum displacement. The maximum displacement of the isolator is 200 mm, obtained from experiments.

2.2. Soil modelling

The two super structures viz. FBNIS and FBBIS are modelled along with the underlying soil. Three-dimensional soil model is made along

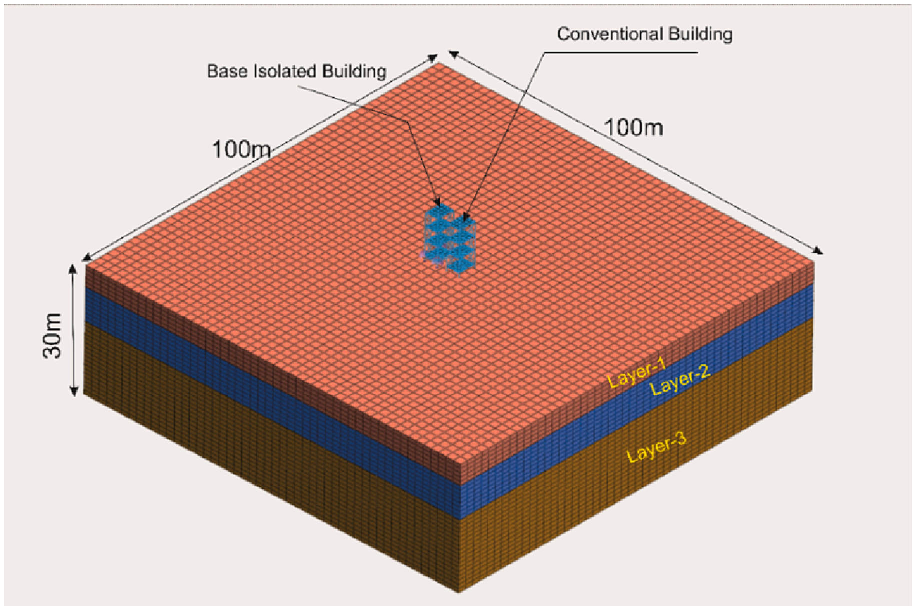

Fig. 6. Finite element configuration used in SSI study.

with the structures, and in SSI, inertial and kinematic interactions, both are considered simultaneously. Fig. 6 shows the FE model of the system. Soil, is modelled as 8 nodded 3D - Brick element. The structures are connected with the soil at one common node and provide an appropriate constraint to ensure equal movement of connected node of soil and structural foundation. 100 m × 100 m by 30 m depth of soil domain is modelled (Fig. 6). SSI analysis using series of nonlinear dynamic time-history analysis in time domain was performed earlier by Sharma et al. [53] considering the optimum size of soil domain and minimization of the reflection of the seismic wave from the boundary. They varied the lateral extents of soil domain along with soil material non-linearity and ground motion PGA and gave a relationship between soil domain length 'L' and width 'W' of the foundation as mentioned in Eq. (1) for higher PGA levels

$$\frac{L}{W} = -0.1W + 11.5 \text{for PGA } > 0.82\text{g} \tag{1}$$

Thus, from the Eq-1, minimum soil domain to foundation width ratio is obtained as 11.5. Roesset and Ettouney [48] also recommended a domain length of 5 W for soils with high internal damping and 10 W–20 W for soils with low internal damping. In the present work, the soil domain length to width of foundation ratio is considered as 22.2 which will give higher accuracy. The soil below the building has three layers of thickness of 5 m, 8 m and 17 m. The layers have shear wave velocity 120 m/s, 250 m/s sand 350 m/s respectively. The average shear wave velocity $V_{s,avg}$ of the soil is 245 m/sec and the fundamental frequency of the soil column is 2.1 Hz.

The mesh density of the soil domain depend on the soil density, small strain shear modulus, element formulation, integration technique and desired maximum frequency of analysis. In case of the soil used in the model, the geometry of the mesh needs to be chosen in such a way that the propagation of shear waves at that frequency is ensured. This will be possible if a mesh type is chosen such that a sufficient number of nodes fit within the minimum shear wavelength. The Lysmer [38] suggested 8 linear elements per wavelength. The minimum soil wavelength size in lateral direction is given by $\lambda_{min} = Vs/f_{max}$. Where is Vs is shear wave velocity of soil and f_{max} is the cutoff frequency of interest, which recommended as 15 Hz (Sharma et. al. 2020) which is more than the 2nd fundamental frequency of the conventional building structure. Lysmer [38] thus recommended that, the size of element will be as mentioned in Eq-2

$$l_{max} \leq \frac{V_s}{8 \times f_{max}} \tag{2}$$

Here, in the present work the shear wave velocity varies from 120 m/s to 350 m/s thus the maximum size of element used considering Eq. (2) is 1 m. As per ASCE (4–16) the dynamic characteristics of the soil are addressed perfectly by maintaining the dimension of the elements smaller than one-fifth of the smallest wavelength (associated with the highest frequency) of interest or cut off frequency. The element size adopted as 1 m, thus also satisfies ASCE 4–16 criteria. In order to avoid reflection of wave from the boundary, free field elements are implemented at the boundary. Further details of soil properties and numerical modelling are available in Bandyopadhyay et al. [11]. Simplified soil model like, Modified Ramberg-Osgood model is used to simulate the nonlinear behavior of soil by a nonlinear shear degradation curve [59]. Small strain shear modulus of soil is obtained from shear wave velocity of the layer using Eq-3.

$$G_{max} = \rho V_s^2 \tag{3}$$

Effect of water table is not considered in the modelling while elastic bedrock is considered at 30 m below the soil layer with a shear wave velocity of 1100 m/sec. The vertical direction and the lateral boundaries of the base are considered rigid. Horizontal input motions are applied at the base of the model at elastic bed rock.

2.3. Validation of numerical model

Validation of the numerical model for linear analysis is required in order to prove its reliability, hence a brief description of the validation with actually measured real earthquake response is mentioned henceforth. The details of numerical analysis and in-depth comparison of structural responses are available in Bandyopadhyay et al. [11]. Buildings were subjected to real earthquakes of very small magnitude. These buildings were instrumented and accelerometers were placed at centre of ground floor and 3rd floor (roof) of the buildings as shown in the Fig. 7. The structural response was recorded on 29th Nov., 2007 earthquake, which occurred at Indo-Myanmar border region at a focal depth of 114.8 km. The local magnitude of this earthquake was 5.1 Mb and distance of epicenter (23.390°N, 94.675°E) from site was 433 km. The response spectra is generated from the recorded floor response time

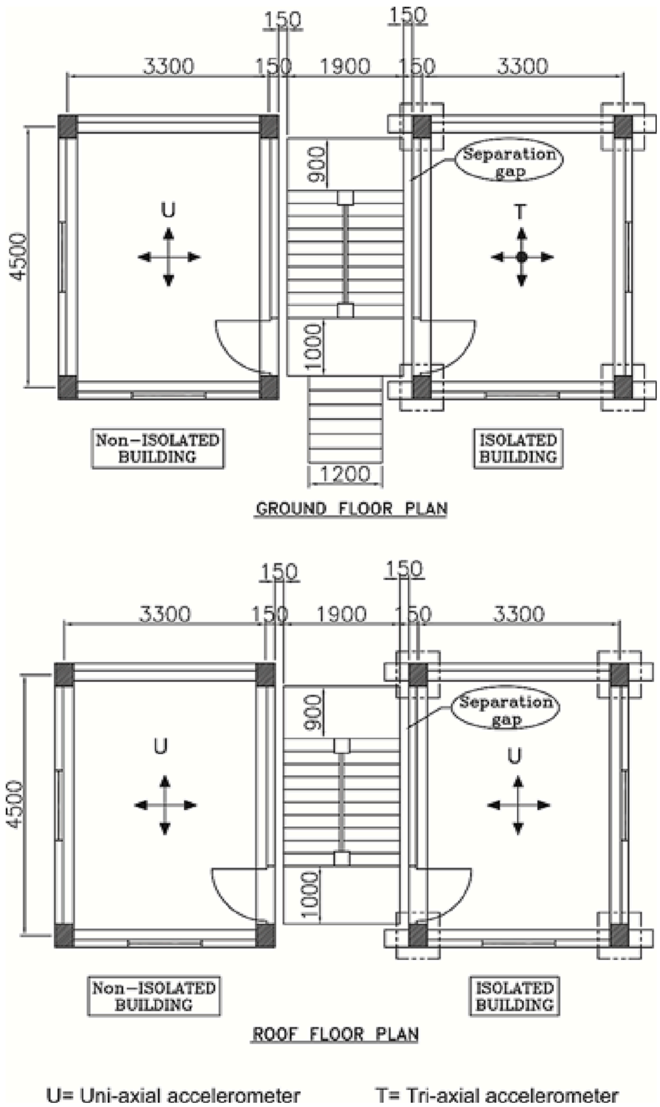

Fig. 7. Position of accelerometers in the prototype conventional and base isolated buildings at ground floor level and Roof level. (after Bandyopadhyay et al. [11].

history. By performing numerical analysis, floor response spectra are also generated at the same level and compared with the recorded spectra. Fig. 8 (a)-(d) show the comparison between actually measured response of the FBBIS and FBNIS during the earthquakes with the response obtained from the numerical analysis of the building for 5% damping. In the location nomenclature, TG represents transverse directional response of ground floor and TR represents transverse directional response of roof. Transverse direction is shorter direction of the building [11]. It is observed that the numerical results predict the performances well in terms of major frequencies. For the FBBIS, the numerical analysis shows two frequencies.The first frequency for the structure with isolator (FBBIS) is 1.9 Hz for both longitudinal and transverse directions.The second frequency is the structural frequency (with foundation soil) and this frequency is obtained numerically as 8.4 Hz and 7.8 Hz in the longitudinal and the transverse directions, respectively. The measured value of first mode frequency for FBBIS is 1.2 Hz for both longitudinal and transverse directions.. The first mode of frequency of the base isolated building is predicted higher than the measured value, which may be due to the uncertainities/variabilities existing in the actual structure and the foundation soil. It is observed that for the FBNIS the predicted peak floor response and the 1st mode of the building are matching with the recorded data, but for the second mode of the structure numerical results predict higher floor spectral acceleration values than the recorded floor response spectrum (FRS) values.. The first and the second frequencies of the FBNIS observed from the numerical model considering foundation soil is 5.05 Hz and 14.38 Hz in the longitudinal direction and 4.74 Hz and 13.25 Hz in the transverse direction. The recorded values are also having similar frequencies as shown in Fig. 8.

2.4. Modelling approaches for nonlinear dynamic analysis

Overall, four approaches are considered for modelling of the non-isolated structures for carrying out nonlinear dynamic analysis when the buildings are subjected to very high ground motions in order to evaluate the fragility functions. In the first approach, nonlinear full soil strata model along with the model of structure and soil explained in the preceding sections is considered. Thus, in this approach nonlinear dynamic analysis is performed on the comprehensive soil model with the structure. This approach is called ***FBNIS-Direct*** approach which is the most realistic approach of modelling. In the second approach, modelling is carried out such that the SSI analyses are performed in two steps.

In 1st step, 1D-site response analysis (SRA) is performed using open-source software, DEEPSOIL considering non-linear behavior of the FE model of the soil and free field motion is evaluated at the free surface. Subsequently, in 2nd step, the obtained free field motion is applied at the base of the structure as a base motion, and soil underlying the structures is represented as an equivalent spring as per ASCE 4–16. This approach is stated as ***FBNIS-SRA*** approach. The third approach is the one in which fixed base analysis is performed simulating that the structure is founded over a rock. This approach is called as Rigid Base Non Isolated Structure-Rock ***(RBNIS-Rock)*** approach. In *RBNIS-Rock* method, input motions at rock outcrop are directly applied at the base of the fixed base structure. The last approach comprises of the structure placed over the soil with Rigid fixed base condition which is termed as ***RBNIS-SRA*** approach. In ***RBNIS-SRA*** procedure, the free field motion obtained by carrying out 1D-SRA is applied at base of the structure with Rigid base. A schematic representation of all the approaches is shown in Fig. 9.

3. Seismic analysis of the structures

Seismic analysis of the structures is carried out by first performing nonlinear static pushover analysis of the structures by considering, rigid (fixed) base condition of the conventional structure. The nonlinear static analysis is performed till failure of the structure to get the inherent characteristics of the structure without soil flexibility effect. Next, free vibration analysis is performed for the above mentioned fixed base structures. Subsequently, the nonlinear dynamic analysis is performed for all the modelling approaches discussed above.

3.1. Capacity curve for the rigid base structure

The pushover analysis of RBNIS is undertaken to have an overall understanding of the nonlinear behaviour of the structure. Before the pushover analysis, the RBNIS is first subjected to gravity loads and static analysis is performed by giving acceleration in vertical direction. The total mass of the structure is 117 Ton. The state of stress from this analysis is saved and subsequently starting from this state the static pushover analysis is conducted in X-direction (Transverse direction) for the fixed base structure. The incremental parabolic lateral forces are applied to the conventional fixed base structure and P-Δ effects are not included in the analysis. The output of a nonlinear static analysis is presented in the form of a 'pushover curve' which is the base shear vs. roof displacement curve and is shown in Fig. 10 for the structure in X-direction. The response of the rigid base structure in terms of the global stiffness and peak strength are 18,043 kN/m and 415 kN respectively. It

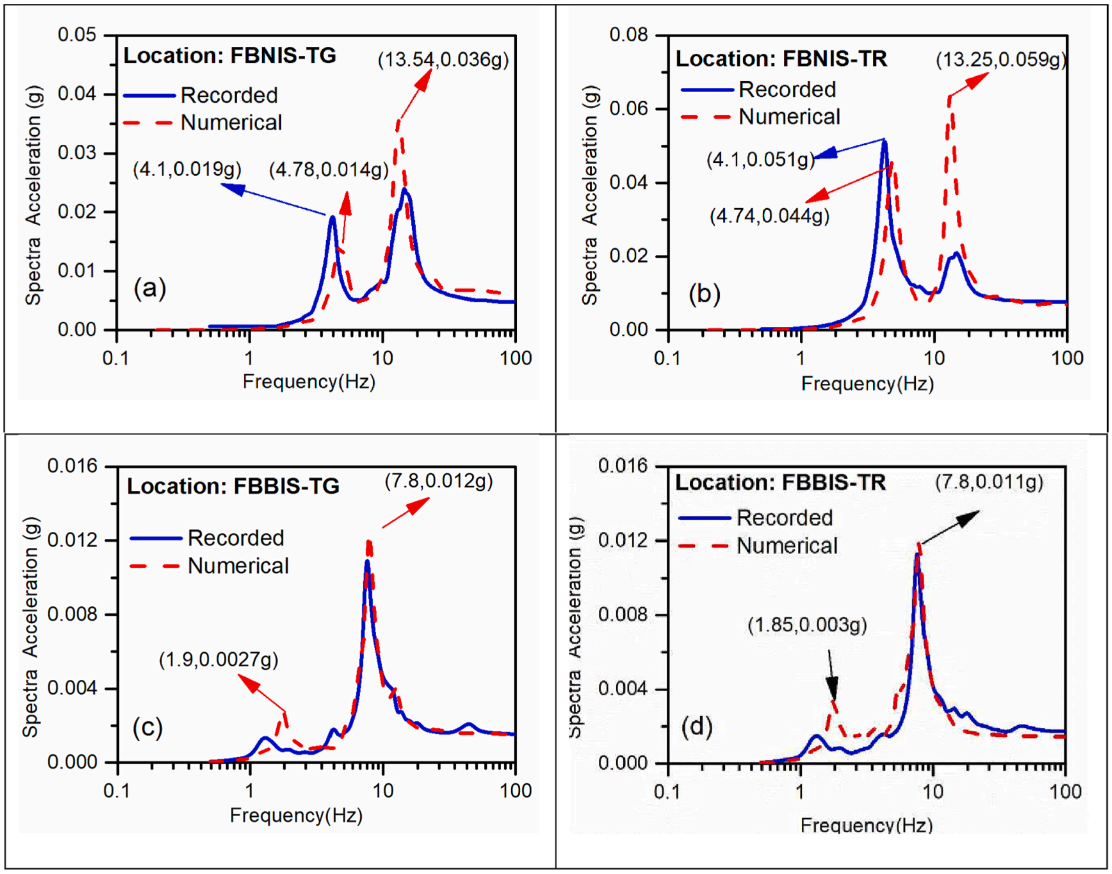

Fig. 8. Comparison of Numerical and measured Transverse directional floor Response spectrum for a)FBNIS Ground floor, b)FBNIS –Roof c) FBBIS- Ground floor, d) FBBIS-Roof (Adopted from Bandyopadhyay et al. [11].

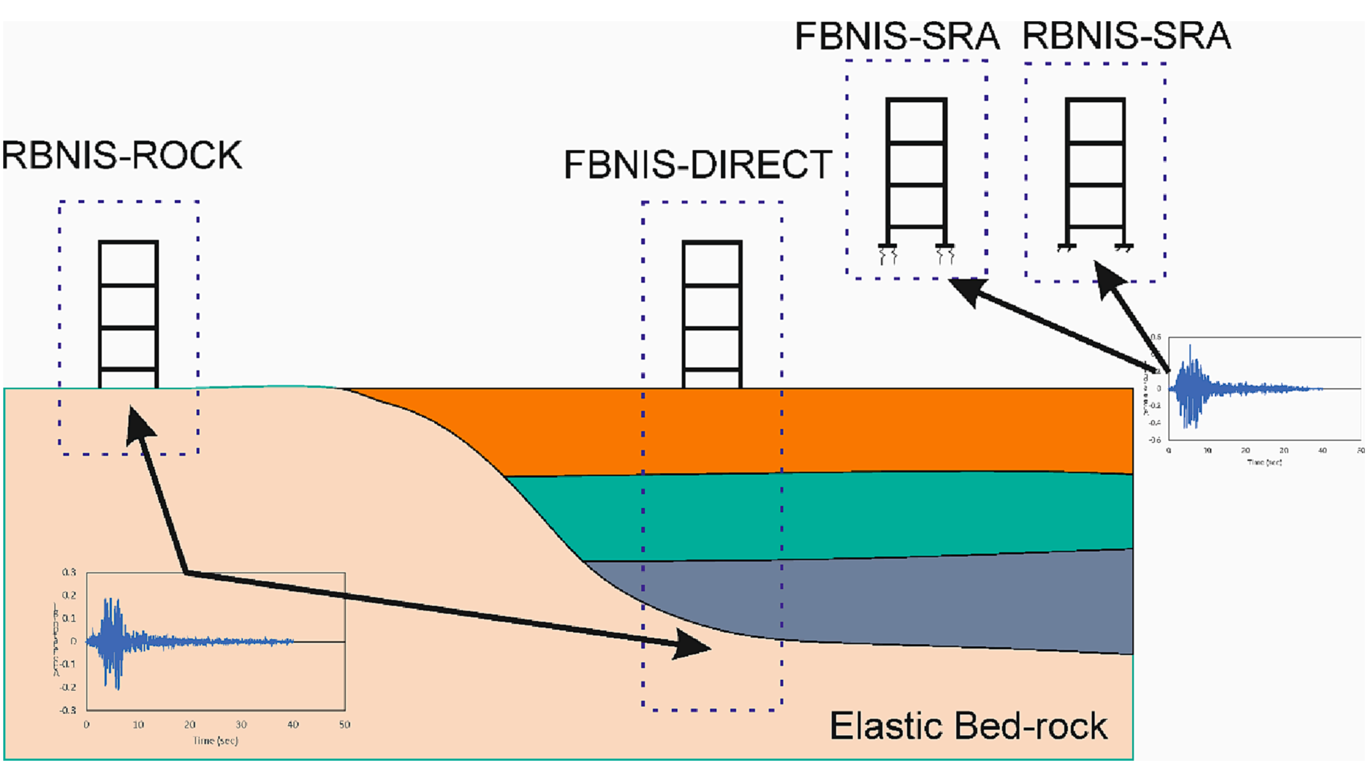

Fig. 9. A schematic representation of different model boundary configurations.

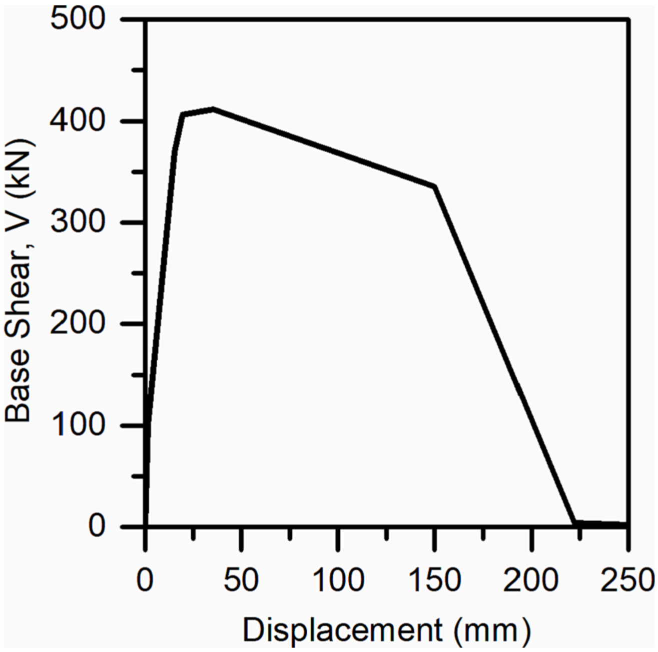

Fig. 10. Pushover curve of the structure for X direction.

can be thus inferred from the capacity curve of the structure that when the structure is subjected to earthquake excitation, the structure will show hysteretic deformation, and reach maximum capacity at about 0.4g PGA. The plastic hinges are initially developed in the columns only and plastic hinges are initiated in the lower story of the building resulting a soft story behaviour.

The fixed base frequency of the RBNIS for longitudinal (Y- Direction) and transverse (X direction) direction are 5.72 Hz and 4.82 Hz respectively. The first mode mass participation factor is more than 90% for both the structures thus demonstrating that the structures are first mode dominated buildings. The free vibration analysis of base isolated structure is performed and, the frequency of this structure is 1.9 Hz and 1.85 Hz for longitudinal (Y direction) and transverse direction (X direction) respectively when fixity is considered below isolator springs.

3.2. Input ground motions

The buildings considered in the present work, are located in Guwahati, India. Though, Guwahati is located in high seismic zone of India, as per authors knowledge no strong motion recorded data is available for Guwahati city. Hence, required earthquake data is to be generated from the artificial histories [18,39] which are required to be compatible with the elastic response spectra defined for the site. In the present study, the representative spectrum compatible ground motion is obtained from uniform hazard response spectra(UHRS) developed for the Guwahati site [10] by employing Probabilistic seismic hazard analysis(PSHA). This target UHRS spectra is generated at the bed-rock level. Spectrum compatible time history of each target spectra are obtained using total time duration, rise time duration, strong motion duration and decay time duration of 20 sec, 5 secs, 10 secs and 5 secs respectively as per EN 1998–1 (2005). The accelerograms are then generated by using SIMQKE [26]program for further use in numerical simulations.

The target artificial spectrum compatible time history is generated using SIMQKE software [26] such that the average root-mean-square deviation (D_{rms}between the generated spectrum and the target spectrum is minimum [Bommer and Acevedo (2004)]. Minimum D_{rms} value signify the closer replication of input motion to the target spectrum. The approach employed in SIMQKE software is to generate a power spectral density function from the smoothed response spectrum, and then to

Table 3
GMPEs used in the present study.

Sr No	GMPE	Tectonic Description	Database	GMPE Nomenclature
1	Akkar et al. [3]	Active Shallow Crustal	Europe and Middle east	GMPE-1
2	NDMA [41]	Active Shallow Crustal	India	GMPE-2
3	Atkinson and Boore [6]	Stable Continental	USA	GMPE-3
4	Sharma et al. [52]	Subduction zone	India and Iran	GMPE-4
5	Pezeshk et al. [44]	Stable Continental	Central and Eastern North America	GMPE-5
6	Singh et al. [56]	Subduction zone	India Nepal	GMPE-6
7	Abrahamson et al. [2]	Active Shallow Crustal	Next Generation Attenuation (NGA) Model	GMPE-7
8	Campbell and Bozorgnia [19]	Active Shallow Crustal	NGA Model	GMPE-8
9	Atkinson and Boore [7]	Active Shallow Crustal	NGA Model	GMPE-9
10	Bozorgnia et al. [15]	Active Shallow Crustal	NGA Model	GMPE-10

derive sinusoidal signals having random phase angles and amplitudes. The sinusoidal motions are then summed and an iterative procedure is used to improve the match with the target response spectrum, by calculating the ratio between the target and actual response ordinates at selected frequencies; the power spectral density function is then adjusted by the square of this ratio, and a new motion is generated. The generated synthetic time history which is compatible to the uniform hazard response spectrum (UHRS) is considered as an input motion.

During PSHA, multiple parameters are taken into consideration such as seismic source characteristics, recurrence law for different earthquake magnitude, seismicity of each zones and median ground motion prediction equation (GMPE) with epicentral distances. A detail pro-

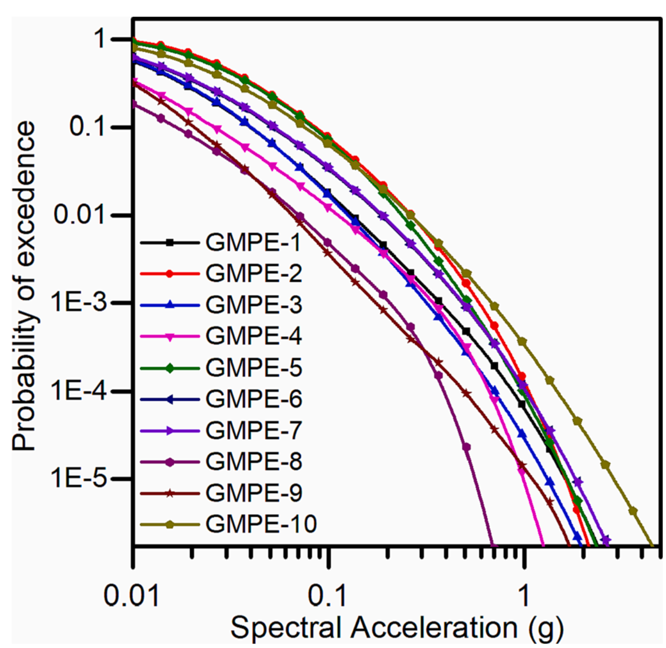

Fig. 11. Variation of POE exceedance of PGA with different GMPEs.

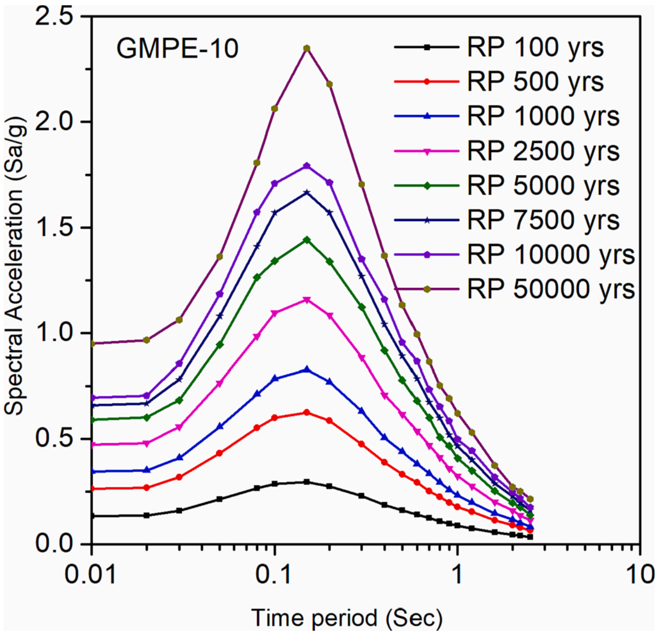

Fig. 12. UHRS target response spectra obtained from PSHA with different return periods for GMPE-10(5 %damped).

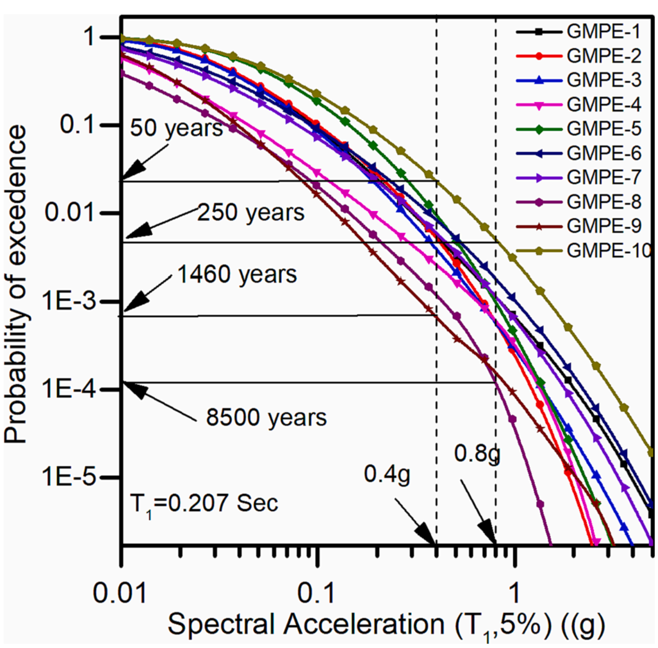

Fig. 13. Hazard Curves showing return period v/s spectral acceleration for different GMPEs at 0.207 time period.

cedure of generation of seismic hazard maps of Assam state is reported in Bandyopadhyay et al. [10]. These maps are created based on seismotectonics, local geology and seismicity of the region by dividing the study area into 10 seismic zones. The maximum credible earthquake magnitude of each zone is evaluated based on Kijko method [34] and method given by Gupta (2002). Attenuation relationships (GMPE) developed by researchers [2,3,6] are employed based on the real earthquakes data or synthetic time histories developed by researchers taking into account local geology. The attenuation equations relate seismic parameter, Y such as PGA, or peak ground velocity (PGV) with earthquake magnitude (M) and distance (r).

$$Y = F(M, r, site)$$

where M represents moment magnitude, and 'r' refers to various types of distances such as epicentral distance, Joyner Boor distance or closest distance. These relationships accounts for the attenuation of seismic energies of a tectonic zone. In the present work, 10 different attenuation relationships (Table 3) referred from the literature are used for the study area.

Hazard curves are then derived from all the ten attenuation relationships and probability of exceedance v/s PGA for all GMPEs are shown in Fig. 11. Similarly, hazard curves are obtained for all time periods from 0.05 secs to 2 secs and then the uniform hazard spectra are then generated at the bedrock level with a shear wave velocity of 1100 m/s for each attenuation relationship corresponding to 50%, 20%, 10%, 5%, 2%, 1%, 0.66%, 0.5% and 0.1%, probability of exceedance in 50 years. Fig. 12 shows the uniform hazard target spectra for different return periods for GMPE-10.

The hazard curves showing probability of exceedance v/s spectral acceleration (5% damped) corresponding to ten different GMPEs at bedrock level for time period of 0.207 sec are shown in Fig. 13. Here, 0.207 sec is the fundamental time period of the structure. It is observed that for earthquakes of different GMPEs at 0.207 s of time period, the return period corresponding to spectral acceleration of 0.4 g ranges from 50 yrs to 1460 yrs. Similarly, for earthquakes of different GMPEs at 0.207 s of time period, the return periods corresponding to spectral acceleration of 0.8 g ranges from 250 yrs to 8500 yrs. The uniform Hazard Response Spectra (UHRS) corresponding to each GMPE for return periods ranging from 50 to 1460 yrs are shown in Fig. 14(a) when the spectral acceleration at 0.207 secs time period for all these earthquakes is 0.4 g. Similarly, UHRS corresponding to each GMPE for return periods ranging from 250yrs to 8500 yrs are shown in Fig. 14(b) when the spectral acceleration at 0.207 secs time period for all these earthquakes is 0.8 g. Thus, it is clear from Fig. 14 that the earthquake acceleration attracted by the structure at 0.207sec time period lies at peak for six out of ten UHRS represented by different GMPEs with a range of return periods. Moreover, when the acceleration attracted by the structure is increased from 0.4 g to 0.8 g, the return period of these earthquakes confirming to different GMPEs also increases.

3.3. Damage measures and intensity measure selection

The damages to the structure associated with the earthquakes is generally defined by the damage measures (DM), which can express the structural response from elastic state to inelastic states. Two different damage measures are considered for two buildings (FBNIS and FBBIS) as one is a conventional structure and the other is base isolated structure. Bhandari et al. [13] studied the effectiveness of various damage measures (DM) for the base isolated building and concluded that maximum isolator displacement is the most appropriate way to represent the building response for the base isolated structure. Hence, in this present study, maximum isolator displacement denoted by D_{max} is considered as a damage measure of base isolated structure (FBBIS). Four different damage states are considered to describe the damage conditions of this building, such as, slight (0.2 D_{max}), moderate (0.4 D_{max}), extensive (0.8 D_{max}) and collapse (1.2 D_{max}) [27]. In the present study, the base isolator is designed with a design displacement of 200 mm, hence this design displacement is considered as maximum isolator displacement (D_{max}). The damage measure frequently used by researchers for FBNIS is the maximum inter story drift ratio (maxIDR) hence the same is considered in the present work for the FBNIS. The selection of intensity measure (IM) is important in describing the earthquake severity and scaling of earthquake records. It describes various characteristics of a seismic ground motion like amplitude, duration, frequency content and energy content. Researchers [55] have used IMs such as peak ground acceleration (PGA), Peak ground Displacement (PGD) and 5% damped Spectral

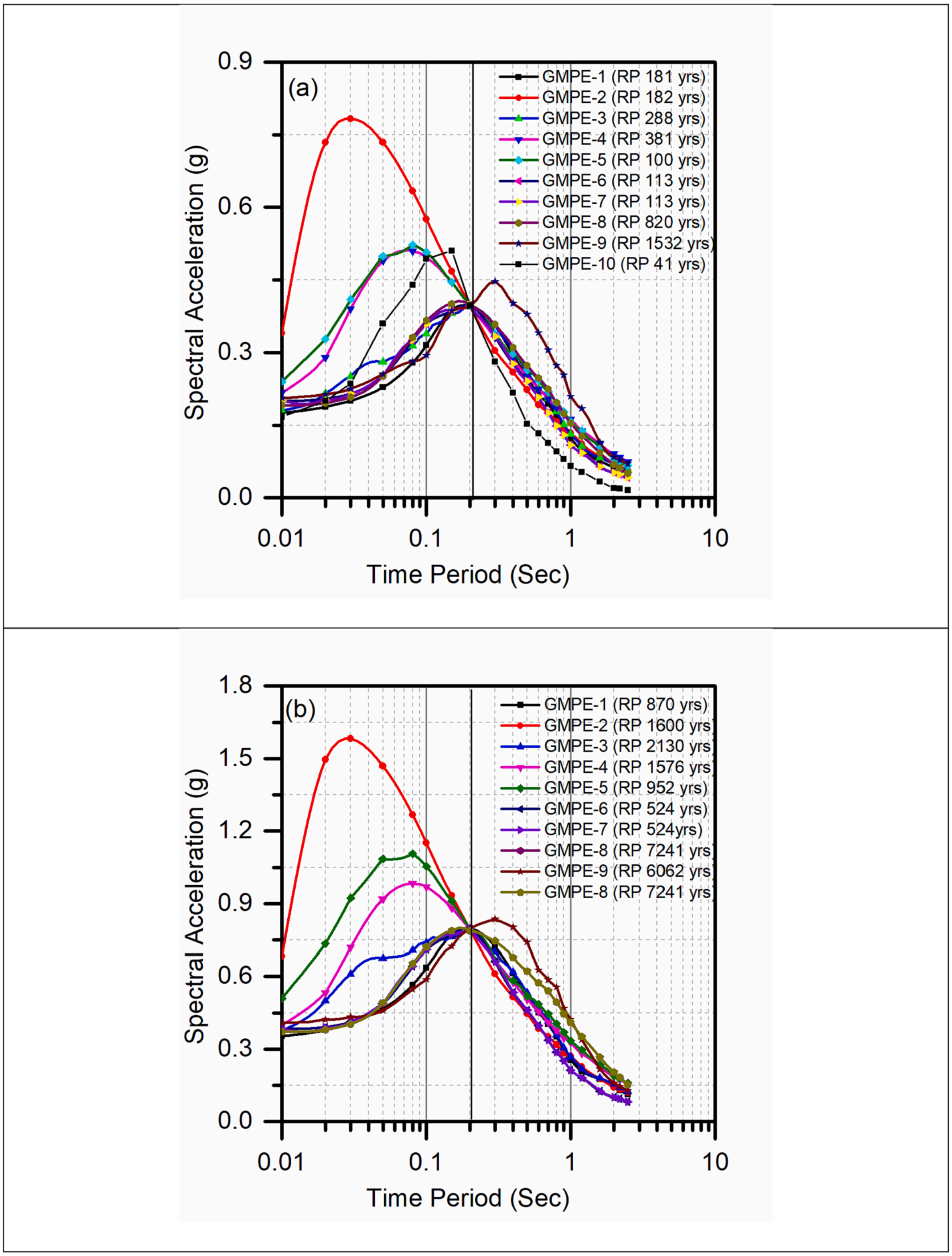

Fig. 14. (a)Response spectra of different GMPEs for different return periods(a) when spectral acceleration for T = 0.207 sec is 0.4 g (b) when spectral acceleration for T = 0.207 sec is 0.8 g.

acceleration at 1st mode ($Sa(T_1)$) [20]. In the present study, two different IMs are selected for the two types of buildings taking into purview their efficiency, practicality and hazard computability [42,46]. Spectral acceleration (5% damped) value at 1st mode is selected as IM for FBNIS and PGA is chosen as an IM for FBBIS due to its low structural frequency.

3.4. Nonlinear time history analysis (NLTHA)

A comparative study is performed depicting the effect of SSI in obtaining building response for the four different modelling configurations of the structure explained in preceding section. 5% Rayleigh's damping was considered for the structure and mass proportional damping coefficient (α) and stiffness proportional damping coefficient (β) of 0.5864 and 0.00106 respectively are input in the analysis. A series of nonlinear time history analyses were conducted on both the structures using spectrum compatible time histories with return periods of 100 yrs, 500 years, 2500 yrs and 50,000 yrs of the target UHRS shown in Fig. 12. The PGA value corresponding to the RPs of 100 yrs, 500 yrs, 2500 yrs and 50,000 yrs are 0.13 g, 0.25 g, 0.43 g and 0.94 g respectively at the rock outcrop. The free field motions are amplified due to the presence of soil and amplified PGA value at the surface level for different

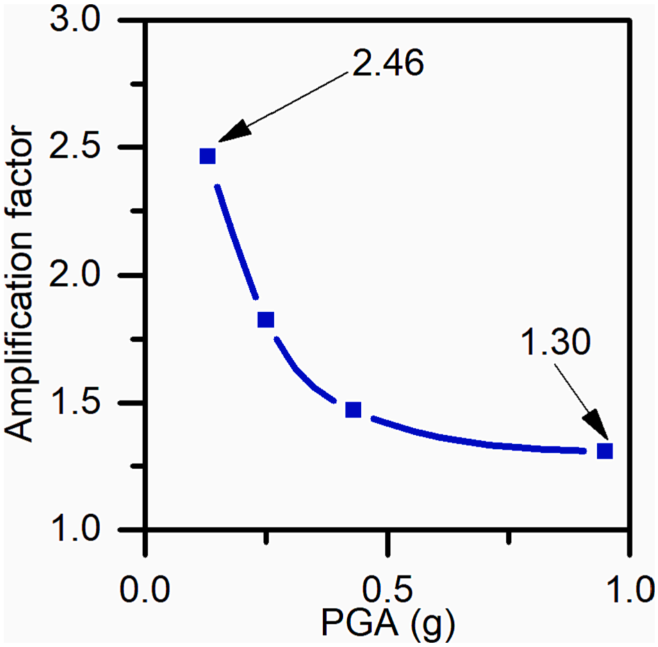

Fig. 15. Amplification factor of base motion during soil response analysis.

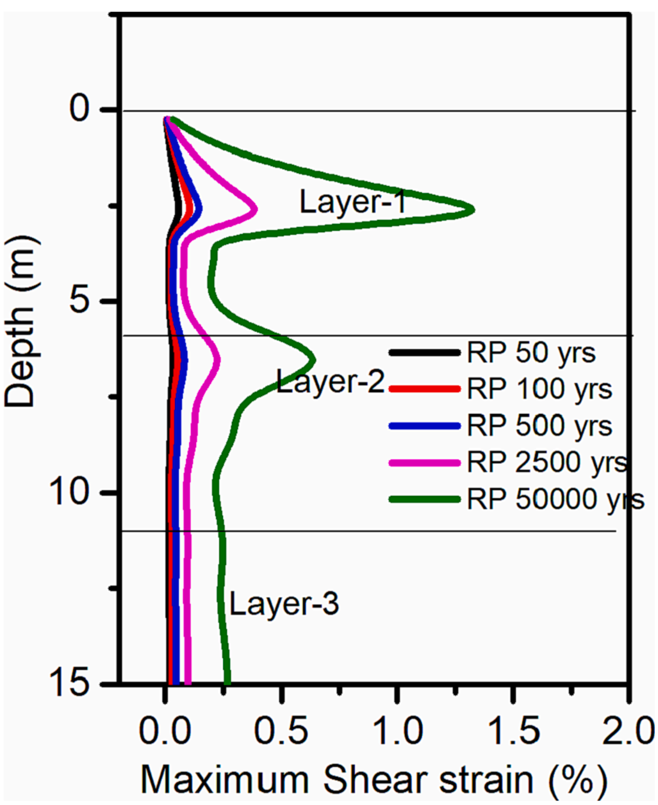

Fig. 16. Variation of soil shear strains with depth for different earthquake intensity level.

RPs of 100yrs, 500yrs, 2500yrs and 50000yrs are observed 0.32 g,0.41 g,0.69 g,1.23 g respectively from nonlinear soil response analysis. The variation of amplification factor (Ratio of surface level PGA to base PGA) is plotted in Fig. 15. It is observed from the figure that the amplification factor of the surface level PGA to rock PGA decreases with increasing earthquake intensity. The possible reason behind this phenomenon is the presence of high soil hysteretic damping for high level of earthquake

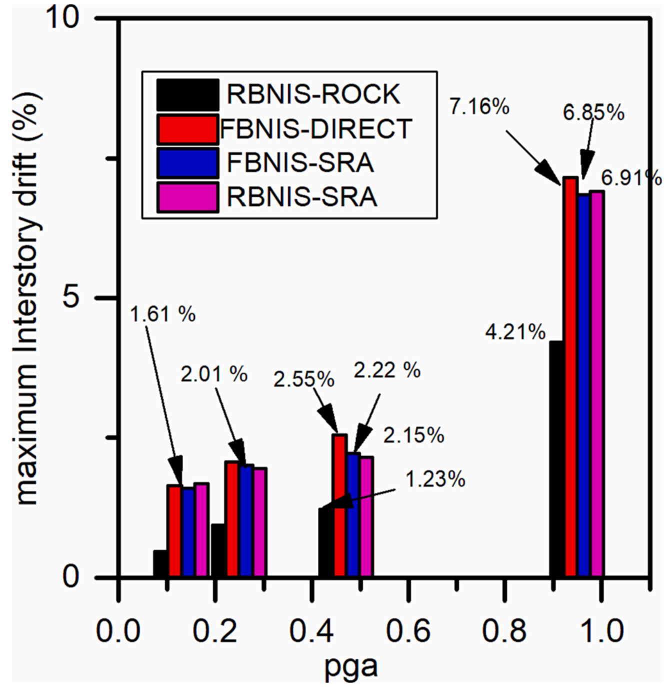

Fig. 17. Variation of maxIDR for different modelling configurations.

intensity. The variation of maximum soil shear strain for different earthquake levels is shown in Fig. 16. It is observed that for earthquake with higher return period the maximum shear strain increases at a depth of 2.5 m and 6.5 m below ground level and this is basically due to large nonlinearity of soil. The damping ratio of soil increases with increasing shear strain and hence the amplification of the motion from bedrock to surface level decreases for earthquakes with large return period or large excitation levels as noticed from Fig. 15.

The structural responses in the form of maximum inter-storey drift (MaxIDR) are obtained from 4 different modelling approaches for the non-isolated structure which are explained in the previous section and their comparison is shown for different PGAs in Fig. 17. The modelling approach of **RBNIS-Rock** shows very less response compared to the others because effects of soil amplification are not considered here. Among all the approaches used, **FBNIS-Direct** method shows higher response and the most accurate response due the incorporation of coupling action between soil and the structure.

The MaxIDR for **FBNIS-SRA** and **RBNIS-SRA** approaches are observed as 6.91% and 6.85% respectively for base spectra of 50000 years return period (RP). Similarly, MaxIDR for these two approaches are observed as 2.22% and 2.15% respectively for base spectra of 2500 yrs RP. The differences may be attributed due to presence of soil spring in **FBNIS-SRA** approach.

Nonlinear dynamic analysis with **FBNIS-SRA** approach and **RBNIS-SRA** approach took 16 times less computational efforts than **FBNIS-Direct** approach with reasonable accuracy. Hence, **FBNIS-SRA** approach is considered for further performing NLTHA and generation of fragility curves with soil and ground motion uncertainties.

The structural response of both the buildings are further studied for different level of input motion intensities using **FBNIS-SRA** modelling approach. The nonlinear response of the column hinges for FBNIS and base isolator deformation of FBBIS when subjected to 4 different target spectra of different RPs of GMPE-10 with increasing excitation levels is studied. Fig. 18 (a-d) represents the moment curvature hysteretic relation of the column hinges and Fig. 18 (e-h) shows the force deformation hysteretic relation of base isolator for different earthquake intensity levels. It is observed that for RP 100 yrs return period which corresponds to 0.125 g PGA (Rock level) the column hinges just enters nonlinear

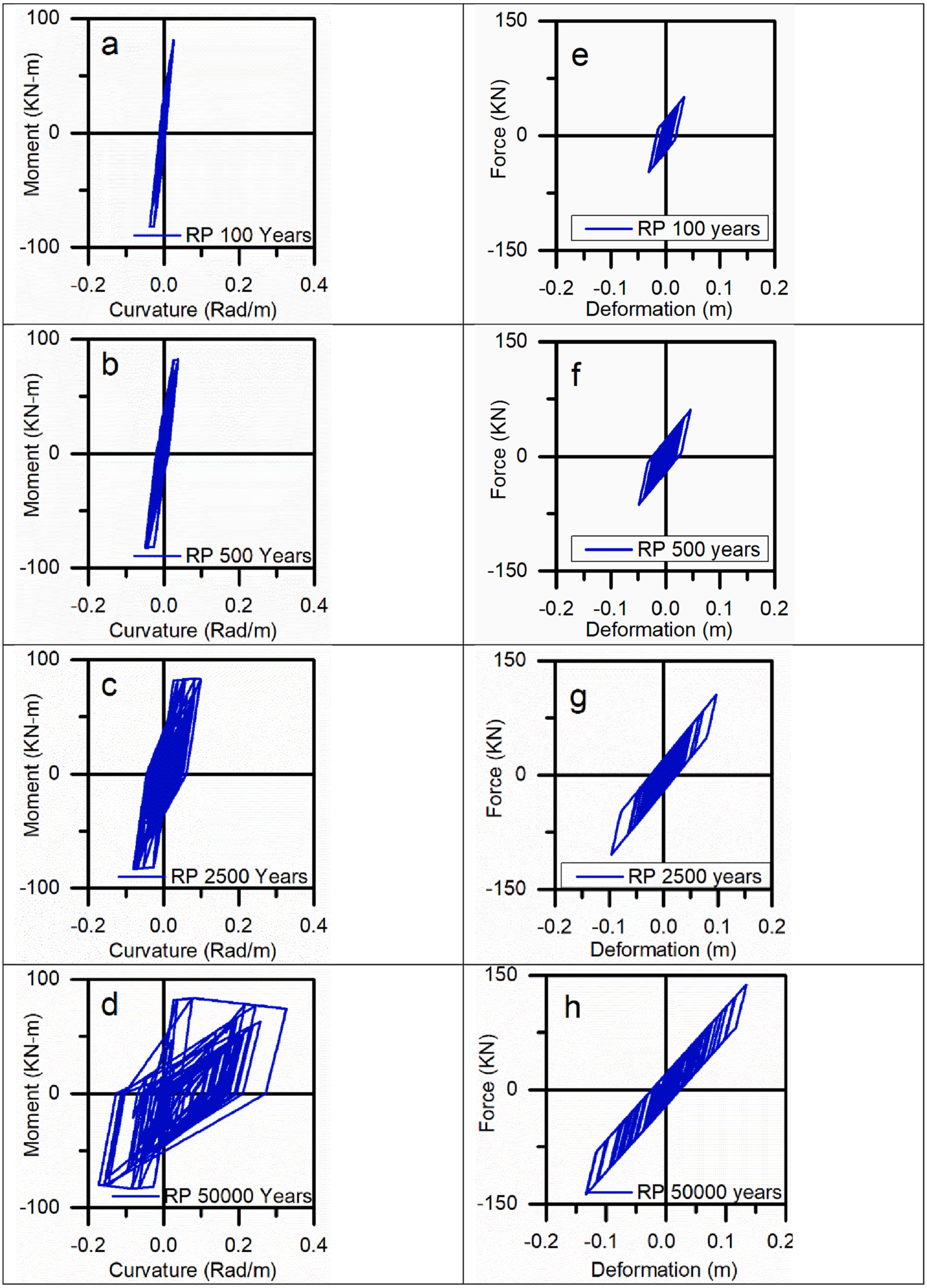

Fig. 18. (a-d) Moment Curvature deformation of column hinges and (e-h) deformation of base isolator displacement for different RPs.

deformation and at 2500 yrs RP spectra which correspond to 0.43 g PGA (at rock level) the column hinges show clear hysteretic deformation. Moreover, when the structure is subjected to spectrum compatible TH of 50,000 yrs RP spectra of 0.94 g PGA (at rock level), the structure show excessive nonlinearity. The nonlinear behavior of base isolated building is observed from 0.125 g PGA to 0.94 g PGA.

4. Seismic fragility analysis

The fragility functions represent the probability that the Damage measure (DM) of a specific structure exceeds a threshold capacity(C) associated with a desired limit state, conditional on the earthquake intensity measure (IM) parameter. Two frequently used analytical procedures to get relationship between structural response (DM) and ground motion parameter (IMs), are Incremental Dynamic Analysis (IDA) [60] and Multiple Stripe Analysis (MSA) [30]. In IDA, the input motions are adopted from the strong motion database or generated from synthetic earthquake, and then scaled linearly to get structural response from linear range to plastic state. These analyses are repeated for a series of input ground motions to gather the structural response for record-to-record variations. Moreover, in the present study soil uncertainties are also considered and analysis is performed for each IGM with different soil parameters like shear wave velocity and plasticity index. In this process, a set of DM values are obtained which are associated with onset the predefined limit state herein described as the inter-story drift that define the threshold of three states (Immediate Occupancy (IO), Life Safety (LS), Collapse Prevention (CP): 1%, 2% and 4%, respectively [1]. The fragility parameters, mean (μ) and lognormal standard deviation (β), are evaluated by taking logarithms of IM with associated predefined limit state. The fragility functions are then constructed using the two-parameter lognormal distribution function. In the present study, it is assumed that all the uncertainties in the fragility curves can be represented as lognormal distributions and it can be plotted by two parameters, such as the lognormal standard deviation (β) and the mean (μ) of the lognormal seismic intensity measure. Probabilistic risk assessment of the structure is performed based on the assessment of log-normal distribution as explained in the following Eq- 5.

$$F_Y(y) = \varnothing\left[\frac{1}{\beta}\ln\left(\frac{y}{\mu}\right)\right] \tag{5}$$

Where, standardized cumulative normal distribution function is represented by $\varnothing$, The standard deviation of natural logarithimic function is β, and mean of logarithmic seismic intensity measure, y, is represented by μ. IDA methods are widely used by researchers [60] for fragility curve generations. Baker and Allin Cornell [9] identified a drawback regarding scaling effects of ground motion during IDA procedure. A significant scaling of IGM scaled the frequency content of the motion at higher intensities, which might not be the actual representation of the motion corresponding to intensity level and consequently may lead to a biased fragility curve. Recently, researchers [10,63] used Multi-Stripe analysis (MSA) procedure for generation of fragility curves. In MSA framework, structural analyses are conducted at discrete set of *IM* levels and different set of IGM can be used for each IM level. Thus it potentially requires a reduced number of structural analyses if *IM* is efficient [16,29]. As all the input motions are different at each *IM* levels, the estimation procedures of fragility parameters are also different and maximum likelihood technique is used. The maximum likelihood estimation methods are used to obtain the two parameters θ_y and β which are mean and standard deviation for characterization of fragility function. The likelihood function ***L*** is expressed in the Eq-6.

$$\boldsymbol{L} = \prod_{j=1}^{k}\left[F_y(a_j)\right]^{x_j}\left[1 - F_y(a_j)\right]^{1-x_j} \tag{6}$$

Where, Specific damage state of a fragility function is represented by $F_y(a_j)$ and x_j is 0 or 1, depending on whether the structure sustains the damage or not. The maximum likely hood estimate is estimated by solving the Eq-7 and Eq-8.

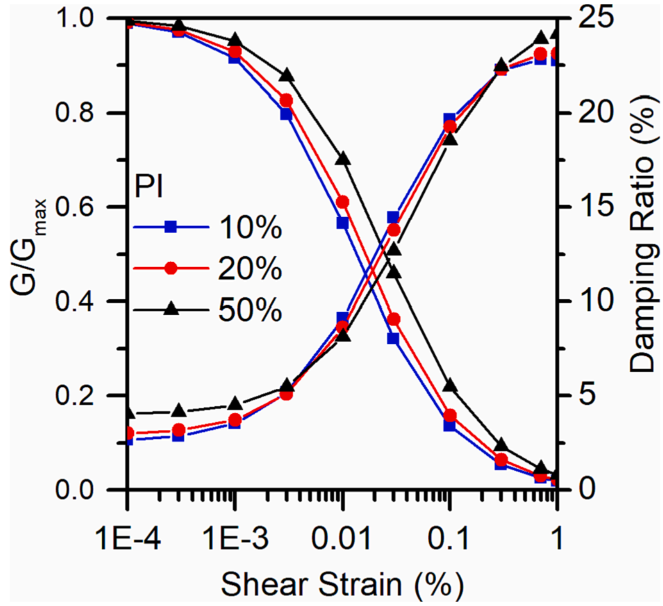

Fig. 19. Variation of shear modulus degradation curve with plasticity index [12].

$$\frac{\partial \ln[L(\theta_Y,\beta)]}{\partial\theta_Y} = 0 \tag{7}$$

$$\frac{\partial \ln[L(\theta_Y,\beta)]}{\partial\beta} = 0 \tag{8}$$

Baker [8] reported that, MSA technique made better estimation of collapse risk in a comparison with IDA methodology provided a valuable information regarding site specific spectra is available. In the present study, MSA technique is used for evaluation of fragility curves of the structure.

4.1. Soil uncertainty

The non-linear dynamic response of the soil subjected to the earthquake depends on the small strain shear modulus(G_{max}) of the soil and shear modulus degradation curves. Dammala and Krishna [23] compared the experimentally obtained G/G_{max} v/s strain and damping ratio v/s strain curve with the curves given by Darendali [24] which are most frequently used from the literature. It was observed this curve given by Darendali [24] under-estimated the experimental shear modulus degradation curve and overestimated the damping ratio curve. Thus, there is lot of uncertainty in the soil strata and this has to be taken care of by considering variation in soil shear wave velocity as well as plasticity index of the soil for evaluation of fragility curves. Uncertainty in shear modulus degradation curves are associated with the soil plasticity index (PI). Hence, three different values of plasticity indices considered in the present work are PI of 10%, 20% and 50%. Moreover, as stated in ASCE 4–16 (2016) soil shear modulus shall be varied between the best-estimate shear Modulus value times (1 + Cv) and the best estimate value divided by (1 + Cv), where Cv is a factor that accounts for uncertainties in the SSI analysis. If insufficient data are available to address uncertainties in soil properties, Cv shall be taken as 1.0. Hence, three different shear modulus of soil are utilized, such as G_{max}, 0.5 times of G_{max} and 2 times of G_{max}, where, G_{max} is the low strain shear modulus of soil which is obtained from the shear wave velocity (V_s) of the soil. The shear wave velocity information is not available for the study area, so the V_s is determined from the empirical relationships between '*SPT -N*

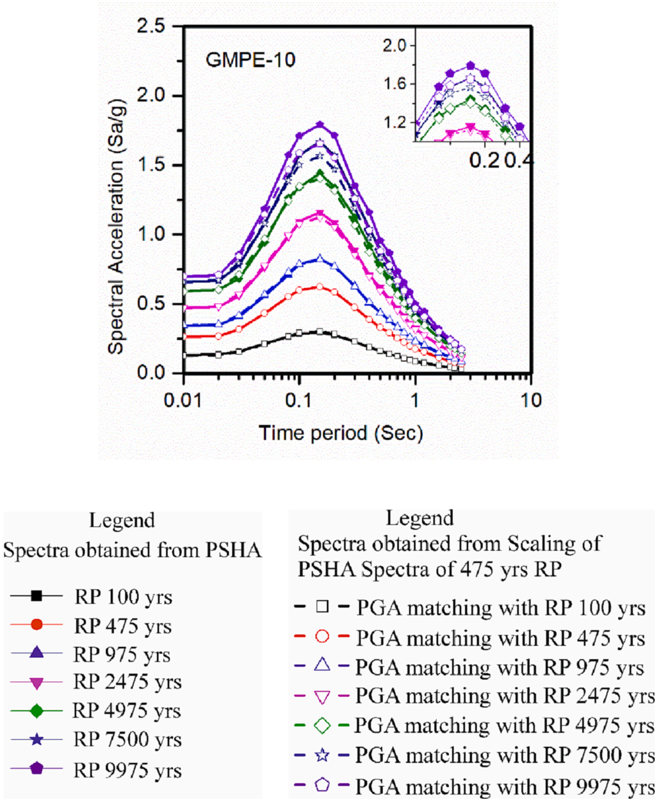

Fig. 20. Comparison of UHRS target response obtained from PSHA for different return period and corresponding scaled spectra at same PGA level.

value – V_s' of soil as reported by Bandyopadhyay et al. [12].

These empirical relationships are developed for soft soil location and are given in Eq-9

$$Vs = 87.18N^{0.32} \text{ (For very soft to clayey silt)} \tag{9a}$$

$$Vs = 41.74N^{0.65} \text{ (For stiff to very stiff silty clay)} \tag{9b}$$

The dynamic soil properties were estimated by Kumar et al. [35]. In general each discretized soil layers have their own shear modulus degradation curve (G/G_{max}) and damping ratio (D) curves depending upon the mean effective confining pressure of that particular layer. The curves showing variation of shear modulus degradation with strain for three different %PI are shown in Fig. 19. The uncertainity in shear modulus of soil is taken into account in the analysis by considering three different shear modulus each with three plasticity indices as discussed above. Accuracy of the MSA technique also depends on the number of earthquake input motions used in each stripe and minimum of ten IGMs were suggested by Sousa et al. [57]. Correspondingly, record to record variation is implemented by applying ten time histories confirming to ten different GMPEs which are obtained by performing PSHA of Assam region [10]. Thus, ninety numbers of NLTHA simulations for each stripe are performed and then Fragility curves are obtained.

4.2. Ground motion uncertainty and scaling

In general, the fragility curves involve significant scaling of original IM to various intensity levels. Proper use of scaling in input ground motion (IGM) required for performing NLTHA is most sensitive part in development of the fragility curve. Herein, a new framework is proposed for ground motion scaling, which is conceptually similar with the existing one but differ in few important points which are not addressed by the researchers till date. In this proposed framework, a site-specific Uniform Hazard response spectrum (UHRS) is used as a target

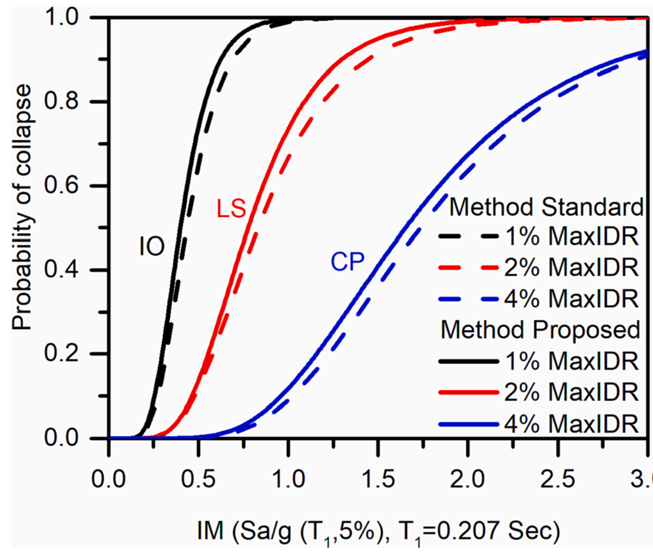

Fig. 21. Fragility curve of the FBNIS (a) Method-Standard, and (b) Method- Proposed.

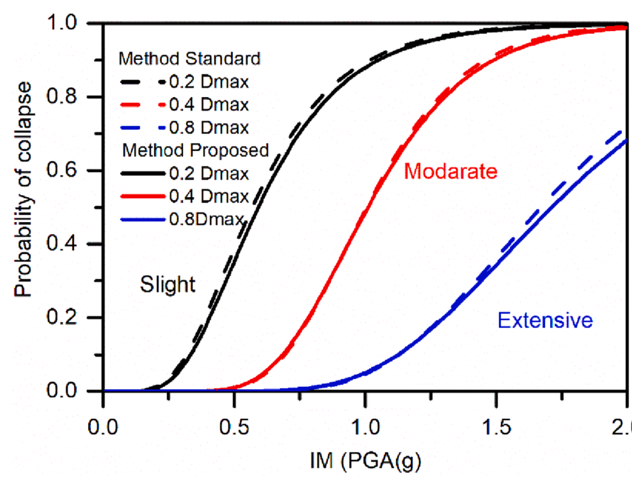

Fig. 22. Fragility curve of the FBBIS (a) Method-Standard, and (b) Method- Proposed.

spectrum which is evaluated with probabilistic seismic hazard analysis (PSHA). The scaling of the spectra is however not done arbitrarily but by using the UHRS generated at different return periods. These represents the scaled spectra and the spectra with higher RP denotes higher ground motion. Ten different GMPEs as explained in previous section are considered for simulating different earthquakes at bed rock level with corresponding ten UHRS. The spectrum compatible artificial time history is generated for each UHRS with corresponding RP using SIMQKE which will give the time history for different levels of seismic intensities. Fig. 20 shows the uniform hazard target spectra for different return periods for GMPE-10. It also shows a conventionally linearly scaled spectra of RP 100 yrs generated to match the PGAs of UHRS with different RPs. It is observed that the conventionally scaled spectra predicted lesser value of spectral accelerations at high intensity level of earthquakes, in the zone of time period of the 1st fundamental frequency of medium rise structure.

The similar phenomenon is noticed for other GMPEs also. So, the advantage of using this proposed procedure of scaling is to simulate the proper frequency content of target spectra and generate more representative and realistic spectra at high input motion intensity levels. The conventional method of scaling and the proposed new methodology of

Table 4
Fragility parameters of FBNIS for the two methods.

Ground motion Scaling method	Fragility Parameter	Immediate Occupancy (IC)	Life Safety (LS)	Collapse Prevention (CP)
Method-Standard	Mean	0.4587 g	0.8319 g	1.73 g
	Std	0.3529	0.4301	0.4113
Method-Proposed	Mean	0.4091 g	0.7768 g	1.6532 g
	Std	0.3487	0.4017	0.4234

scaling are the two methods used for scaling of IM to various intensities and subsequently generate fragility curves for limit states of IO, LS and CP. The fragility curves generated by linear scaling of UHRS of 100 yrs RP carried out as per conventional approach is denoted by *Method-Standard* and fragility curves obtained from the proposed new methodology of ground motion scaling using UHRS of higher RP are denoted as *Method-Proposed*.

5. Results and discussions

The fragility curves pertaining to three different limit states for the FBNIS (shown in Fig. 21) and FBBIS (shown in Fig. 22) with reference to different ground motion scaling (*Method-Standard* and *Method-Proposed*) are described here and explained for seismic vulnerability assessment. The mean and lognormal standard deviation values related to different limit states for both the methodologies for FBNIS are reported in Table 4 considering 5% damped first modal spectral acceleration as IM. The mean value generated by *Method-Standard* is larger than the mean value generated by *Method-Proposed* at all limit states, which indicates that the building evaluated by *Method-Proposed* is more vulnerable than that

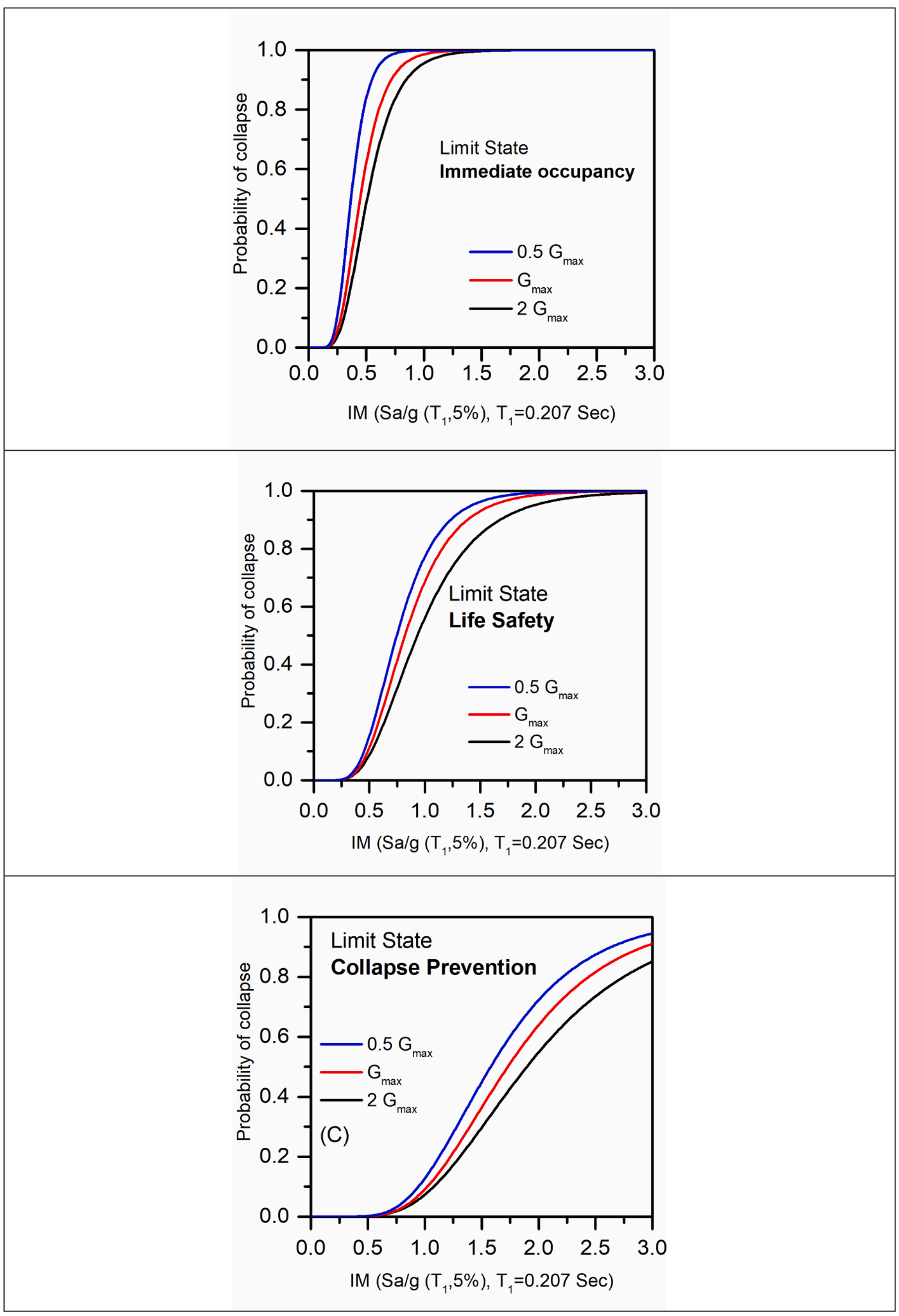

Fig. 23. Variation of fragility curve of different limit states for different soil conditions for FBNIS.

evaluated by *Method-Standard.* It is also observed from Fig. 21, that the fragility curve generated by the *Method-Proposed* shows higher probability of failure of structure compared to the *Method-Standard*. The probability of collapse of the structure is 42% based on *Method-Proposed* while it is 36% based on *Method-Standard* for the life safety (LS) limit state of the structure with reference to IM (which is 5% damped first mode spectral acceleration) of 1.5 g. Hence, the buildings are 6% more vulnerable to the seismic collapse when the proposed method is used especially at higher spectral acceleration. For lower level of IM, such as IM = 0.6 g, both the methods show similar probability of collapse of the building at all three limit states. The possible reason behind this observation is that the peak of target spectra obtained from linear scaling adopted by Method-Standard is underestimated than that obtained by Method-Proposed for the same PGA at higher intensities of earthquake level (Fig. 20). At 5% damped spectral acceleration of 0.9 g (or PGA of 0.36 g) corresponding to maximum credible earthquake of the Guwahati site (IS1893-2016), the Probability of Exceedance (POE) of structure for limit state of LS is 66% using *Method-Proposed and* 58% using conventional *Method-Standard*. Similarly, the POE is 98% and 8% respectively for limit state of IO and CP using *Method-Proposed* while it is 96% and 6% for limit state of LS and CP using *Method-Standard.* This shows high seismic vulnerability of the structures for PGA of 0.36 g. This is because the structures are designed for Design basis earthquake with PGA of 0.18 g (IS1893-2016) and with response reduction factor of 3. The response reduction factor considered for the structure is 3 which based on AERB siting code [AERB/NF/SC/S] and it suggests to adopt a response reduction factor of 0.67 times the value of response reduction factor defined in [14]-2016 for general industrial buildings with ductile detailing.

Fig. 22 shows the fragility curve for the FBBIS for various performance limit states using both the methodologies. No significant differences are observed in the fragility parameters for the base isolated building by adopting both *Method -Standard* and *Method-Proposed.* This may be due to the following reasons. It is known that more than 95% mass is participated in the 1st mode of structure in base isolated structure. The *Method -Standard and Method-Proposed* both give same acceleration of the structure at higher time period of 1–2 s (lower frequency) and hence the displacement of the base isolated building will be same when both *Method -Standard* and *Method-Proposed are* used.

Fig. 23 depicts the variation of fragility curves for different soil conditions for FBNIS. SSI has an effect on the seismic assessment of the structures for all the limit states for FBNIS. Three different shear modulus of soil are considered for fragility assessment and soil with low shear modulus is more vulnerable than other cases. Soil corresponding to the low shear wave velocity shows higher deformation due to soil nonlinearity, and thus shows higher probability of failure.

6. Conclusions

A novel methodology of generation of fragility curve using spectrum compatible time histories through PSHA with realistic scaling of IGMs is presented in this paper. The seismic fragility analysis has been carried out for the two instrumented midrise structures (one is flexible base non isolated structure (FBNIS) and other is Flexible base Base-Isolated structure(FBBIS)) using the proposed technique of scaling and standard method of linear scaling. Soil uncertainty has been incorporated by considering variation in shear modulus of soil and variation in the plasticity indices of the soil. The following conclusions are drawn from the work carried out.

1. Fragility functions are evaluated for the FBNIS by modelling the structure with soil springs and applying free field motion obtained from soil amplification studies at the support of the springs as it gives computationally efficient results. It is also noticed that neglecting soil structure interaction (SSI) produces 2.6 times lesser structural response acceleration value than that obtained by considering SSI.
2. The midrise structure yields at a lateral load of 40 tons and when FBNIS is subjected to earthquake with a surface level peak base excitation of 0.4 g, it has a maximum inter storey drift of 1.5% and shows small hysteretic deformation of the columns while the structure when it is subjected 0.95 g peak base excitation, it shows high nonlinearity in hinges of the columns with maximum inter-storey drift of 6%.
3. The Uniform Hazard Response Spectra generated from ten GMPEs demonstrate that as the return period of the UHRS increases, the acceleration attracted by the structure confirming to earthquakes of these different GMPEs also increases and that all the 10 GMPEs used have different spectral peaks at different frequencies.
4. Soil uncertainty incorporated in Fragility curves shows that soil corresponding to the low shear wave velocity ($0.5G_{max}$ value of shear modulus) shows higher deformation due to soil nonlinearity, and thus shows higher probability of failure than the soil having shear modulus of $2G_{max}$ for all the three limit states of Immediate Occupancy (IO), Life Safety (LS) and Collapse Prevention (CP).
5. The proposed methodology (*Method-Proposed*) of scaling of UHRS based on RP gives 5% to 10% more vulnerable POE fragility values for all the three limit states of IO, LS and CP than the *Method-Standard* of linear scaling of GMs especially at high spectral accelerations (IMs) above 1 g. However, both the methods show comparable POE values at all three limit states for IM lower than 0.6 g. No significant differences are observed in the fragility parameters for the base isolated structure by implementing both the methods. This proposed methodology thus can be used for assessment of the medium rise structure where there is lack of real earthquake data.

Declaration of Competing Interest

The authors declare that they have no known competing financial interests or personal relationships that could have appeared to influence the work reported in this paper.

References

[1] 356, F. 2000. Prestandard commentary for the seismic rehabilitation of buildings. DC (FEMA Publication No. 356, Washington.
[2] Abrahamson NA, Silva WJ, Kamai R. Summary of the ASK14 ground motion relation for active crustal regions. Earthq Spectra 2014;30:1025–55.
[3] Akkar S, Sandıkkaya MA, Bommer JJ. Empirical ground-motion models for point- and extended-source crustal earthquake scenarios in Europe and the Middle East. Bull Earthq Eng 2014;12:359–87.
[4] Andrade RB, Pereira EM, Cavalcante GH, Vieira Jr LC, Siqueira GH. Seismic fragility assessment for a RC building in seismically stable Brazil: a sensitivity analysis. J Build Eng 2022;60:105184.
[5] Andreotti G, Calvi GM. Nonlinear soil effects on observed and simulated response spectra. Earthquake Eng Struct Dyn 2021;50:3831–54.
[6] Atkinson GM, Boore DM. Earthquake ground-motion prediction equations for eastern North America. Bull Seismol Soc Am 2006;96:2181–205.
[7] Atkinson GM, Boore DM. The attenuation of Fourier amplitudes for rock sites in Eastern North America. Bull Seismol Soc Am 2014;104:513–28.
[8] Baker JW. 2013. Trade-offs in ground motion selection techniques for collapse assessment of structures. *Vienna Congress on Recent Advances in Earthquake Engineering and Structural Dynamics*, Vienna.
[9] Baker JW, Allin Cornell C. A vector-valued ground motion intensity measure consisting of spectral acceleration and epsilon. Earthquake Eng Struct Dyn 2005;34:1193–217.
[10] Bandyopadhyay S, Parulekar YM, Sengupta A. Generation of Seismic Hazard maps for Assam region and incorporation of the Site effects. Acta Geophys 2022;70(5):1957–77.
[11] Bandyopadhyay S, Parulekar Y, Sengupta A, Chattopadhyay J. Structure soil structure interaction of conventional and base-isolated building subjected to real earthquake. Structures Elsevier 2021:474–93.
[12] Bandyopadhyay S, Sengupta A, Reddy GR. Development of correlation between SPT-N value and shear wave velocity and estimation of non-linear seismic site effects for soft deposits in Kolkata city. Geomech Geoeng 2021;16(1):1–19.
[13] Bhandari M, Bharti S, Shrimali M, Datta T. Seismic fragility analysis of base-isolated building frames excited by near-and far-field earthquakes. J Perform Constr Facil 2019;33:04019029.
[14] BIS. 1893. Criteria for earthquake resistant design of structures. Bureau of Indian Standards, Part, 1.

[15] Bozorgnia Y, Stewart JP, Kishida T, Boore DM, Campbell KW, Atkinson GM, et al. Response to Discussion by P. Malhotra on "NGA-West2 Research Project". Earthq Spectra 2015;31:1879–84.
[16] Bradley BA. A generalized conditional intensity measure approach and holistic ground-motion selection. Earthquake Eng Struct Dyn 2010;39:1321–42.
[17] Bradley BA. A critical examination of seismic response uncertainty analysis in earthquake engineering. Earthq Eng Struct Dyn 2013;42(11):1717–29.
[18] Cacciola P, Zentner I. Generation of response-spectrum-compatible artificial earthquake accelerograms with random joint time–frequency distributions. Probab Eng Mech 2012;28:52–8.
[19] Campbell KW, Bozorgnia Y. NGA-West2 ground motion model for the average horizontal components of PGA, PGV, and 5% damped linear acceleration response spectra. Earthq Spectra 2014;30(3):1087–115.
[20] Caprili S, Nardini L, Salvatore W. Evaluation of seismic vulnerability of a complex RC existing building by linear and nonlinear modeling approaches. Bull Earthq Eng 2012;10:913–54.
[21] Ciampoli M, Pinto PE. Effects of soil-structure interaction on inelastic seismic response of bridge piers. J Struct Eng 1995;121:806–14.
[22] Dabiri H, Faramarzi A, Dall'Asta A, Tondi E, Micozzi F. A machine learning-based analysis for predicting fragility curve parameters of buildings. J Build Eng 2022;62:105367.
[23] Dammala P, Krishna AM. Nonlinear seismic resposne analysis in northeastern India considering the comprehensive dynamic soil behavior. Indian Geotech J 2022;52:650–74. https://doi.org/10.1007/s40098-022-00598-z.
[24] Darendali M. Development of new family of normalized modulus reduction and material damping. University of Texas; 2001. PhD.
[25] Echeverria MJ, Jünemann R, Liel AB. Seismic fragility assessment of medium-rise fishbone-type reinforced concrete wall buildings. J Build Eng 2022;59:105044.
[26] Gasparini, D.A. 1976. Simulated earthquake motions compatible with prescribed response spectra-SIMQKE. A computer program distributed by NISEE.
[27] Gong W, Xiong S. Probabilistic seismic risk assessment of modified pseudo-negative stiffness control of a base-isolated building. Struct Infrastructure Eng 2016;12:1295–309.
[28] Iervolino I, Cornell CA. Record selection for nonlinear seismic analysis of structures. Earthq Spectra 2005;21:685–713.
[29] Iervolino I, Giorgio M, Galasso C, Manfredi G. Conditional hazard maps for secondary intensity measures. Bull Seismol Soc Am 2010;100:3312–9.
[30] Jalayer F, Cornell C. Alternative non-linear demand estimation methods for probability-based seismic assessments. Earthquake Eng Struct Dyn 2009;38:951–72.
[31] Karapetrou S, Fotopoulou S, Pitilakis K. Seismic vulnerability assessment of high-rise non-ductile RC buildings considering soil–structure interaction effects. Soil Dyn Earthquake Eng Struct Dyn 2015;73:42–57.
[32] Kent DC, Park R. Flexural members with confined concrete. J Struct Div 1971;97:1969–90.
[33] Khosravikia F, Mahsuli M, Ghannad MA. The effect of soil–structure interaction on the seismic risk to buildings. Bull Earthq Eng 2018;16:3653–73.
[34] Kijko A. Estimation of the maximum earthquake magnitude, m max. Pure Appl Geophys 2004;161:1655–81.
[35] Kumar SS, Krishna AM, Dey A. Dynamic properties and liquefaction behaviour of cohesive soil in northeast India under staged cyclic loading. J Rock Mech Geotech Eng 2018;10:958–67.
[36] Lin T, Harmsen SC, Baker JW, Luco N. Conditional spectrum computation incorporating multiple causal earthquakes and ground-motion prediction models. Bull Seismol Soc Am 2013;103(2A):1103–16.
[37] Lopez-Caballero F, Gelis C, Regnier J, Bonilla L. 2012. Site response analysis including earthquake input ground motion and soil dynamic properties variability. 15WCEE, LISBOA.
[38] Lysmer J. 1978. Analytical procedures in soil dynamics. NASA STI/Recon Technical Report N, 80, 12243.
[39] Mitropoulou CC, Lagaros ND, Papadrakakis M. Generation of artificial accelerograms for efficient life-cycle cost analysis of structures. Eng Struct 2015;88:138–53.
[40] Mylonakis G, Gazetas G. Seismic soil-structure interaction: beneficial or detrimental? J Earthq Eng 2000;4:277–301.
[41] NDMA. 2010. Development of probabilistic seismic hazard map of India. Govt of India, New Delhi.
[42] Nielson BG, DesRoches R. Seismic fragility methodology for highway bridges using a component level approach. Earthquake Eng Struct Dyn 2007;36:823–39.
[43] Ouyang X, Zhang Y, Ou X, Shi Y, Liu S, Fan J. Seismic fragility analysis of buckling-restrained brace-strengthened reinforced concrete frames using a performance-based plastic design method. Structures Elsevier 2022:338–50.
[44] Pezeshk S, Zandieh A, Campbell KW, Tavakoli B. Ground-motion prediction equations for central and eastern North America using the hybrid empirical method and NGA-West2 empirical ground-motion models. Bull Seismol Soc Am 2018;108:2278–304.
[45] Pitilakis K, Karapetrou S, Fotopoulou S. Consideration of aging and SSI effects on seismic vulnerability assessment of RC buildings. Bull Earthq Eng 2014;12:1755–76.
[46] Porter K, Kennedy R, Bachman R. Creating fragility functions for performance-based earthquake engineering. Earthq Spectra 2007;23:471–89.
[47] Raychowdhury P. Effect of soil parameter uncertainty on seismic demand of low-rise steel buildings on dense silty sand. Soil Dyn Earthquake Eng 2009;29:1367–78.
[48] Roesset JM, Ettouney MM. Transmitting boundaries: a comparison. Int J Numer Anal Meth Geomech 1977;1:151–76.
[49] Sáez E, Lopez-Caballero F, Modaressi-Farahmand-Razavi A. Inelastic dynamic soil–structure interaction effects on moment-resisting frame buildings. Eng Struct 2013;51:166–77.
[50] Sathurshan M, Thamboo J, Mallikarachchi C, Wijesundara K. Seismic fragility of lightly reinforced concrete school building typologies with different masonry infill configurations. Structures Elsevier 2023:1710–28.
[51] Scozzese F, Tubaldi E, Dall'Asta A. Assessment of the effectiveness of Multiple-Stripe Analysis by using a stochastic earthquake input model. Bull Earthq Eng 2020;18:3167–203.
[52] Sharma ML, Douglas J, Bungum H, Kotadia JJ. Ground-motion prediction equations based on data from the Himalayan and Zagros regions. J Earthq Eng 2009;13:1191–210.
[53] Sharma N, Dasgupta K, Dey A. Optimum lateral extent of soil domain for dynamic SSI analysis of RC framed buildings on pile foundations. Front Struct Civ Eng 2020;14:62–81.
[54] Shi Y, Xiong L, Qin H, Han J, Sun Z. Seismic fragility analysis of LRB-isolated bridges considering the uncertainty of regional temperatures using BP neural networks. Structures Elsevier 2022:566–78.
[55] Shome N, Cornell CA, Bazzurro P, Carballo JE. Earthquakes, records, and nonlinear responses. Earthq Spectra 1998;14:469–500.
[56] Singh S, Arroyo D, Srinivas D, Suresh G. Ground motion prediction equation for earthquakes along the Western Himalayan arc. Curr Sci 2021;120.
[57] Sousa L, Silva V, Marques M, Crowley H. On the treatment of uncertainties in the development of fragility functions for earthquake loss estimation of building portfolios. Earthquake Eng Struct Dyn 2016;45:1955–76.
[58] Stewart JP, Fenves GL, Seed RB. Seismic soil-structure interaction in buildings. I: Analytical aspects. J Geotech Geoenv Engrg 1999;125:26–37.
[59] Szilvágyi Z, Ray RP. Verification of the Ramberg-Osgood material model in Midas GTS NX with the modeling of torsional simple shear tests. Periodica Polytechnica Civil Eng 2018;62:629–35.
[60] Vamvatsikos D, Cornell CA. Incremental dynamic analysis. Earthquake Eng Struct Dyn 2002;31:491–514.
[61] Vamvatsikos D, Cornell CA. Applied incremental dynamic analysis. Earthquake Spectra 2004;20:523–53.
[62] Vamvatsikos D, Cornell CA. Direct estimation of seismic demand and capacity of multidegree-of-freedom systems through incremental dynamic analysis of single degree of freedom approximation. J Struct Eng 2005;131:589–99.
[63] van der Burg L, Kohrangi M, Vamvatsikos D, Bazzurro P. A risk-based evaluation of direct displacement-based design. Bull Earthq Eng 2022:1–23.